JOURNAL OF SOLID STATE CHEMISTRY 108, 314–335 (1994)

Structural Considerations and High Resolution Electron Microscopy Observations on $La_nTi_{n-\delta}O_{3n}$ ($n \geq 4\delta$)

G. Van Tendeloo,* S. Amelinckx,* B. Darriet,† R. Bontchev,† J. Darriet,† and F. Weill†

*EMAT, University of Antwerp (RUCA), Groenenborgerlaan 171, B2020 Antwerp, Belgium; and †Laboratoire de Chimie du Solide du CNRS, Université de Bordeaux 1, 33405 Talance Cedex, France

Received February 12, 1993; accepted June 3, 1993

Crystals of the compounds $La_nTi_{n-\delta}O_{3n}$ are shown, by means of electron diffraction and high resolution electron microscopy, to form a homologous series of hexagonal or rhombohedral structures. The structures can be described as resulting from the perovskite structure by the periodic introduction of intrinsic stacking faults in a cubic stacking of close packed LaO_3 layers. The titanium ions, which have mixed valencies, occupy the octahedral interstices between the close packed LaO_3 layers, whereas the interstices in the fault planes remain vacant, making up for the nonstoichiometry. The corner-sharing TiO_6 octahedra are found to be cooperatively tilted about the normal to the layer planes. The "cut and projection" method is used to analyze the electron diffraction patterns and to determine the stacking sequences from geometrical features of the diffraction patterns. Six different stacking sequences are confirmed by direct imaging. High resolution images support the tilt scheme of the TiO_6 octahedra. The formation mechanism of the regular block sequences is discussed and the defects which allow this mechanism to operate are modeled and visualized.

1. INTRODUCTION

Several ternary oxides containing lanthanum and titanium have been characterized in the La–Ti–O system with a La/Ti ratio equal to 1. In most of them the titanium ion is tetravalent (1). Recently a study of the $LaTiO_x$ system reported on a series of layered titanium oxides structurally related to the perovskites (2).

$LaTiO_{3.5}$ (= $La_2Ti_2O_7$ with all Ti^{4+}), known for several years (3, 4), is a member ($n = 3$) of a homologous series of layered structures (5–7) $A_nB_nO_{3n+2}$ ($0 \leq n < \infty$) based on the variation in thickness of the component perovskite slabs of distorted TiO_6 octahedra. By changing the oxygen stoichiometry a new phase $LaTiO_{3.4}$ (= $La_5Ti_5O_{17}$ with titanium valency smaller than 4) was, together with the $n = 4$ compound, the first conducting member of this series. The structure of this new phase was determined from high resolution electron microscopy (HREM) data supported by X-ray and thermogravimetric analysis (8). In the range $3.4 < x < 3.50$ well-ordered intergrowth takes place between the $n = 4$ and the $n = 3$ compounds. This study confirms that the most interesting transport and magnetic properties are expected for compounds in which titanium occurs in a mixed-valence state (titanium valencies +4 and +3).

$LaTiO_3$ is a compound with Ti valency +3 whose structure is a distorted orthorhombic perovskite ($GdFeO_3$ structure) (9, 10).

Elsewhere hexagonal perovskite-like structures with general formula $xA_4B_3O_{12} + yA'B'O_3$ (A and A' = La, Ca, Sr, Ba and B and B' = Ti, Nb, W) have been reported (11–16). In the La–Ti–O system the crystal structure of $La_4Ti_3O_{12}$ is based on the close packed stacking of LaO_3 layers and corresponds to the 12R hexagonal polytypoid with a hcch sequence (h = hexagonal stacking; c = cubic stacking) along the c-axis.

Previous results have shown that $La_4Ti_3O_{12}$ reacts easily with ABO_3 compounds (A = Ca, Sr, Ba; B = Ti, Ru) (14, 15). These materials are structurally related to hexagonal structures and belong to the homologous series $A_nLa_4Ti_3B_nO_{12+3n}$ ($n = 0, 1, 2$), where all the B-cations are present with a formal valence state +4.

As the difference between the ionic radii of Ti^{4+} (0.0601 nm) and Ti^{3+} (0.067 nm) is not large it seemed interesting to synthesize $La_nTi_{n-1}O_{3n}$ phases that can be regarded as belonging to the $La_4Ti_3O_{12}$–$LaTiO_3$ system. In these compounds the titanium is present in a mixed valence state corresponding to +4 and +3. For this reason some interesting physical properties can be expected for these compounds with layered structures.

2. EXPERIMENTAL

The compounds of the $La_nTi_{n-1}O_{3n}$ system have been prepared by solid state reactions of $La_4Ti_3O_{12}$ and $LaTiO_3$. Starting materials were weighed and mixed; after grinding, the powder was pressed into pellets. These pellets were sintered under vacuum at 1073 K for 8 hr and subse-

0022-4596/94 $6.00

quently at 1673 K for 8 hr. All the products were slowly cooled to room temperature. Previously the preparations of $La_4Ti_3O_{12}$ and $LaTiO_3$ were performed from appropriate mixtures of La_2O_3 + Ti_2O_3 heated under vacuum and La_2O_3 + TiO_2 fired in air respectively.

Bulk structural analysis was carried out by X-ray powder diffraction with Cu$K\alpha$ radiation. The data of X-ray diffraction powder patterns have been refined by the Rietveld method (17). These results have been published elsewhere (24).

High resolution electron microscopic observations were made on freshly powdered samples deposited on holey carbon films or on copper grids dipped in a soft glue. Observations were made using a 400-kV microscope with a point resolution of 0.17 nm. The electron diffraction experiments, exploring reciprocal space, were performed on the same type of samples using a 200-kV instrument.

3. STRUCTURAL CONSIDERATIONS

The materials with chemical compositions $La_nTi_{n-\delta}O_{3n}$ form a homologous series of mixed layer compounds consisting of a framework of LaO_3 close packed layers the geometry of which is shown in Fig. 1a. Within the layers the lanthanum and oxygen atoms are ordered in such a way that each lanthanum atom is surrounded by six oxygen atoms, whereas each oxygen atom has two lanthanum atoms among its six nearest neighbors. The sublattice of lanthanum atoms thus forms a hexagonal array with lattice parameter a_H = 5.57 Å. Stacking of these layers occurs in such a way that the lanthanum atoms are as widely separated as possible; i.e., the lanthanum positions in one layer project along the normal to the layer in the center of a triangle formed by the lanthanum atoms in the adjacent layer. The stacking of such layers (ignoring the oxygen atoms), can thus be described by the usual stacking symbols *ABC* . . . or cc . . . hh . . . , depending on whether one wishes to emphasize the layer positions or the stacking mode. It should be noted that the stacking symbols are assumed to bear on the lanthanum arrangement only, i.e., on close-packed layers with omissions.

One third of the octahedral interstices between two such layers are surrounded exclusively by oxygen atoms; they are occupied by titanium atoms (Figs 1b, 1c). However, due to the actual composition, in particular to the cation deficiency, not all octahedral interstices can be occupied. It was shown in (14) that the stacking of LaO_3 layers is of the type hcc . . . ch and that the titanium deficiency is accommodated as complete layers of vacant octahedral interstices. These layers are located in the midplanes of the quadruplets of layers resulting from the two adjacent hexagonally stacked triplets such as $A\gamma B$ ❑ $A\gamma B$, where γ stands for a layer of oxygen octahedral sites partially filled by titanium atoms according to Fig.

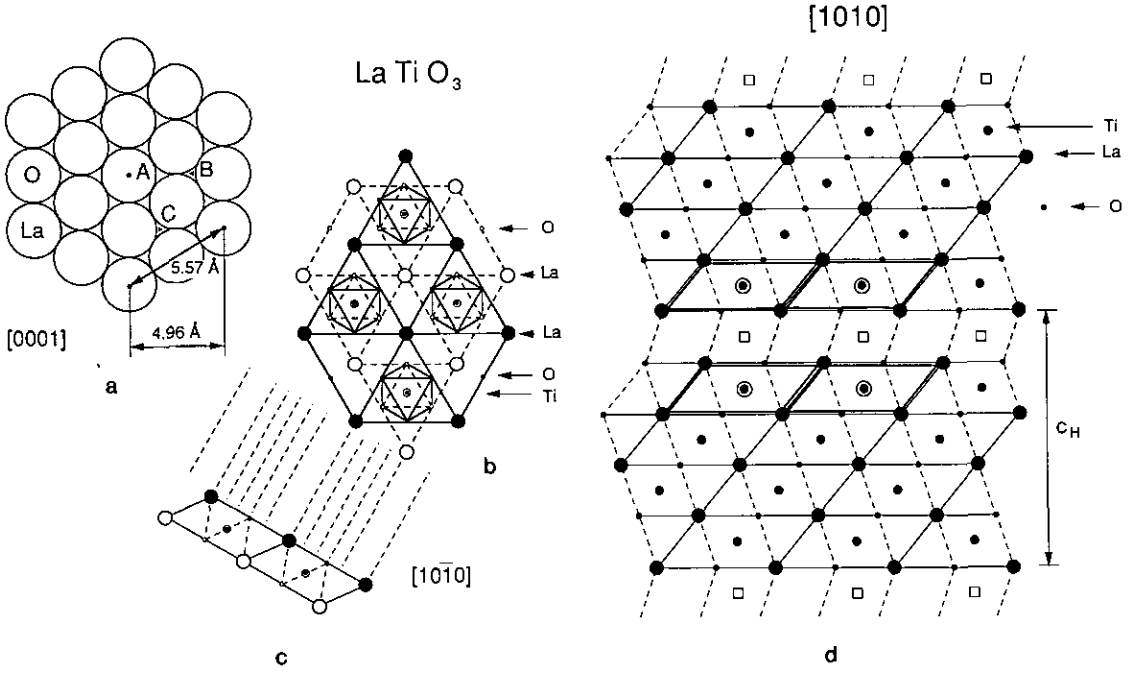

FIG. 1. Schematic representation of the structure of the compounds $La_nTi_{n-1}O_{3n}$. (a) Arrangement of lanthanum and oxygen atoms in the LaO_3 layers parallel to (0001). (b) Sandwich of LaO_3 close packed layers showing the octahedral interstices occupied by titanium ions, LaO_3–Ti–LaO_3. (c) View of (b) along the close packed rows of atoms. (d) Schematic representation of the 10H structure of $La_5Ti_4O_{15}$ as viewed along the close packed rows of columns. This schematic representation can be compared with the image of Fig. 12b.

1b and ❑ for a layer of vacant octahdral sites. The stacking symbol of the stoichiometric compound $LaTiO_3$ would be $A\gamma B\alpha C\beta$ . . . , but due to the nonstoichiometry the full stacking symbol of the compound $La_4Ti_3O_{12}$ would for instance be

$$B\gamma A \square B\gamma A\beta C\alpha B \square C\alpha B\gamma A\beta C \square A\beta C\alpha B \ldots$$

(A,B,C: LaO_3 layers; α,β,γ: Ti- layers; ❑ vacant layers). For the subsequent discussion it is convenient to describe the structure as consisting of identical blocks separated by vacancy layers, successive blocks being displaced over a vector $\frac{1}{3}[11\bar{2}0]_H$ (Fig. 1d).

If the chemical composition is represented by $La_nTi_{n-1}O_{3n}$ ($n \geq 4$) the number of LaO_3 layers in each block is n and that of titanium layers is $n - 1$. If the number n is a (threefold $-$ 1) the resulting stacking has a repeat period along the layer normal which contains a single block and the structure is hexagonal. If the number n is a threefold or a (threefold + 1) the stacking only repeats after three blocks and the structure is rhombohedral. These considerations are only valid in the simplest case considered here, i.e., for the composition $La_nTi_{n-1}O_{3n}$; they are generalized in the following paragraph.

4. BUILDING PRINCIPLES

Assuming the above-mentioned building principles to be obeyed, it is evident that the number of vacancy-containing layers must increase with increasing cation deficiency. For instance, if the composition is $La_nTi_{n-\delta}O_{3n}$ (δ = small integer) the number of vacancy containing layers in the repeat unit should become δ and consequently also the number of "blocks". The repeat unit meant here may have a thickness equal to the c_H-parameter in some cases; in other cases it may be $c_H/3$, depending on the value of n (mod 3), as discussed above. It is possible to formulate the block sequence for a compound of a given composition obeying the described stacking principle.

For simplicity we first consider integer values of δ only. Let the chemical composition be given by $La_nLi_{n-\delta}O_{3n}$. The three numbers n, $n - \delta$, $3n$ are supposed not to have any common factor. We further accept as an empirical fact that blocks of two different sizes are sufficient to generate any composition, provided the compositions of these blocks are of the form $La_mTi_{m-1}O_{3m}$ and $La_{m+1}Ti_mO_{3(m+1)}$, where m is chosen in such a way that the cation deficiency of the compound, i.e. δ/n is intermediate between those of the two blocks; i.e. one must have $1/m + 1 < \delta/n < 1/m$ or the equivalent double inequality

$$m < n/\delta < m + 1. \qquad [1]$$

From a suitably chosen mixture of two such blocks the desired average composition can always be achieved. We shall show how the relative abundancies $p/(p + q)$ and $q/(p + q)$ of the two block sizes (m and $m + 1$) can be computed given the average composition (i.e. given n and δ).

One must clearly have

$$pm + (m + 1)q = n \qquad [2]$$

$$(m - 1)p + mq = n - \delta \qquad [3]$$

$$3pm + 3q(m + 1) = 3n, \qquad [4]$$

where (2) and (4) are in fact equivalent relations. From (2) and (3) we deduce

$$m(p + q) = n - q \qquad [5]$$

$$m(p + q) = n - \delta + p \qquad [6]$$

and hence

$$\delta = p + q. \qquad [7]$$

Moreover

$$p = (m + 1)\delta - n \qquad [8]$$

$$q = n - m\delta. \qquad [9]$$

The possibility for the formation of this homologous series is based on the mixed valence of titanium, but limitations on the chemical formula follow from the requirement for charge compensation. In the limiting case where all titanium atoms were in the Ti^{3+} state the composition would have to be $LaTiO_3$, since La is always in the La^{3+} state and O in the O^{2-} state. On the other hand, should all the titanium atoms be in the Ti^{4+} ionization state, the composition would have to be $La_4Ti_3O_{12}$. Only compositions which are intermediate between these two limiting compositions can lead to a stable structure of the type described here. The chemical composition can thus also be formulated as a linear combination of the two extreme ones:

$$N\ LaTiO_3 + M\ La_4Ti_3O_{12} \quad \text{or} \quad La_{N+4M}Ti_{N+3M}O_{3N+12M}.$$

The nonstoichiometry is then defined by $\delta = (N + 4M) - (N + 3M) = M$ with $\delta \geq 1$ for compounds of the considered series. This means that $M \geq 1$; the lower limit for n in the formula $La_nLi_{n-\delta}O_{3n}$ is thus $n \geq 4$.

Another way of stating this requirement is to consider the La/Ti ratio. This has to be intermediate between that in $LaTiO_3$, La/Ti = 1, and that in $La_4Ti_3O_{12}$, i.e., La/Ti = 4/3. This leads to an upper limit for δ,

$$1 < n/(n - \delta) \leq 4/3;$$

i.e., to

$$0 < \delta \leq n/4. \qquad [10]$$

The two inequalities (1) and (10) severely limit the number of compounds that can be expected as stable phases.

Examples of applications:

(1) $La_9Ti_7O_{27}$ $n = 9; \delta = 2$
$4 < 9/2 < 5$ $m = 4$
$p = 1$ $q = 1.$

The block sequence is an alternation of 4 and 5 layer blocks; the "repeat unit" can be formulated as 45.

(2) $La_{17}Ti_{13}O_{51}$ $n = 17; \delta = 4$
$4 < 17/4 < 5$ $m = 4$
$p = 3$ $q = 1$

The block sequence thus consists of an alternation of three four-layer blocks followed by one five-layer block; the repeat unit is now 4445.

In the first case the unit cell contains three repeat units; the resulting structure is rhombohedral. In the second case the unit cell contains one repeat unit and the structure is hexagonal since 17 = threefold − 1.

5. SYMMETRIES OF THE MULTIBLOCK PHASES

We noted above that if the composition is $La_nTi_{n-1}O_{3n}$ ($\delta = 1$) all blocks, separated by vacancy layers, are equally thick and contain n LaO_3 layers and $(n - 1)$ Ti layers. The repeat unit then contains one such block and its size is equal to the c-parameter if the structure is hexagonal. If the structure is rhombohedral the c-parameter contains three repeat units. The symmetry of the structure, H, R_-, or R_+ was shown to depend on n, if

n = threefold − 1: H
n = threefold: R_+
n = threefold + 1: R_-,

where R_+ means that successive repeat units of the rhombohedral stacking have their first layers stacked in the succession *ABC*, whereas R_- means that this succession is *CBA*.

From the geometrical construction, to be discussed below (Sections 6 and 7), which is used to determine the block sequences it follows that the minority blocks always occur in isolation and if $\delta \leq 4$ there is only one minority block in the repeat sequence. Since the minority and the majority blocks differ in thickness by one LaO_3 layer, the two-block repeat units such as 54, 65, . . . can only belong to one of the three categories

(i) one hexagonal (h) and one rhombohedral block (r_+)
(ii) one hexagonal (h) and one rhombohedral block (r_-)
(iii) one r_+ and one r_- block.

The combination h + h is not compatible with the stacking rules because either the number of layers must be the same for both blocks, and in that case h h is equivalent to h, or the two blocks must differ by three layers, and this is against the stacking principle that implies that the blocks can only differ in thickness by one layer.

Writing down the explicit letter sequences it can, for instance, be concluded that the structure resulting from a repeat unit consisting of one hexagonal block and one rhombohedral r_+ block results in a rhombohedral R_+ structure. In shorthand:

$$h + r_+ \Rightarrow R_+$$
$$h + r_- \Rightarrow R_-$$
$$r_+ + r_- \Rightarrow H.$$

For "three-block" repeat units six combinations have to be considered, none of them leading to a hexagonal structure. In order to show this we first deduce simple combination rules which make it possible to reduce complicated sequences to the three mentioned two-block cases. We note that $2r_-$ changes the stacking position *A* into *C* and hence is equivalent to r_+; in short $2r_- \Rightarrow r_+$. Similar reasoning leads to the following relations:

$2r_- \Rightarrow r_+$ $3r_+ \Rightarrow h$ $n\,h \Rightarrow h$
$2r_+ \Rightarrow r_-$ $3r_- \Rightarrow h.$

For the six three-block combinations one finds by reduction, for instance;

$h + 2r_+ \Rightarrow h + r_- \Rightarrow R_-$ $2r_- + r_+ \Rightarrow r_+ + r_+ \Rightarrow R_-$
$h + 2r_- \Rightarrow h + r_+ \Rightarrow R_+$ $2h + r_- \Rightarrow h + r_- \Rightarrow R_-$
$2r_+ + r_- \Rightarrow r_- + r_- \Rightarrow R_+$ $2h + r_+ \Rightarrow h + r_+ \Rightarrow R_+$

This last relation, for instance, can be illustrated explicitly as follows:

ABCAB/ABCAB/ABCABC//BCABC/BCABC/BCABCA//CABCA/CABCA/ . . .
5h 5h $6r_+$ 5h 5h $6r_+$ 5h 5h

. . . CABCAB//
$6r_+$

We now consider the "four-block" repeat units. Due to the fact that the minority block can only appear once and only if $\delta \leq 4$, there are only six possibilities which can be reduced in the following ways:

$3h + r_+ \Rightarrow h + r_+ \Rightarrow R_+$ $\quad h + 3r_+ \Rightarrow h + h \Rightarrow H$
$3h + r_- \Rightarrow h + r_- \Rightarrow R_-$ $\quad r_- + 3r_+ \Rightarrow r_- + h \Rightarrow R_-$
$h + 3r_- \Rightarrow h + h \Rightarrow H$ $\quad r_+ + 3r_- \Rightarrow r_+ + h \Rightarrow R_+.$

The following combinations could apparently lead to further possible structures: $2h + 2r_+$ and $2h + 2r_-$. However, if these combinations are to be compatible with the stacking principles we must have that:

(i) In such a symbol the hexagonal blocks have the same number of layers since otherwise their thickness would differ by three, which has to be excluded.

(ii) The two rhombohedral blocks have the same number of layers since otherwise one would have three different block thicknesses in the repeat unit, which we excluded.

(iii) We can thus only have a symbol of the form *xxyy* (e.g., 5566 or 5544), where the total number of layers $n = 2x + 2y$ is necessarily even and where also the number of blocks in the repeat unit, which is δ, is even as well, since it is 4. The chemical formula $La_nTi_{n-\delta}O_{3n}$ can thus be simplified by deviding all subscripts by 2.

In conclusion, the symbol $2h + 2r_\pm$ can be simplified to $h + r_\pm$ and the block sequence is *xy* (56, or 54). This is a general feature: symbols in which a common numerical factor occurs lead to a chemical composition in which the same common factor is present. According to our basic rules this common factor has to be removed before applying the algorithms that determine the stacking.

It is easy to verify that the "cut and projection" method (18–20) applied for instance to $La_{22}Ti_{18}O_{66}$ leads to the sequence 5656, which is equivalent to 56. (This is also reflected in the chemical composition which can be simplified to $La_{11}Ti_9O_{33}$).

If the number of blocks (i.e., δ) becomes larger than 4, complicated sequences containing the minority blocks more than once, but still in isolation, may occur, e.g., 44545, which is the sequence corresponding to $La_{22}Ti_{17}O_{66}$.

The simple algorithms discussed above make it possible to deduce the symmetry of the structure generated by an arbitrary sequence of blocks by progressive reduction. Consider, for example, the sequence 44545 belonging to the type $r_- r_- h r_- h$; we successively have

$$r_- r_- h r_- h \Rightarrow r_+ h r_- h \Rightarrow r_+ r_- h \Rightarrow hh \Rightarrow H.$$

The resulting structure is thus hexagonal, as can be verified directly on the explicit stacking symbol:

ABCA/CABC/ BCABC/BCAB/ABCAB/A
4 4 5 4 5

6. GENERALIZATION

We now generalize the considerations of the previous paragraph 4 and 5 to arbitrary values of δ. The cation deficiency is defined by the formula $La_nTi_{n-\delta}O_{3n}$, where δ may now adopt nonintegral, even irrational values.

The average spacing between vacancy layers must now be n/δ. This average spacing must be equal to the average block size, which is given by $[mp + (m + 1)q]/(p + q)$, where p and q are the numbers of m-layer blocks and $(m + 1)-$layer blocks, respectively, in a sufficiently long sequence; i.e., $p/(p + q)$ and $q/(p + q)$ are the relative abundancies of the two block types. We thus must have

$$n/\delta = [mp + (m + 1)q]/(p + q) \text{ or}$$
$$[(n/\delta) - m]p + [n/\delta - (m + 1)]q = 0. \quad [11]$$

It is possible to map each block sequence on a 2D lattice with a rectangular unit mesh of $m \times (m + 1)$ units. Assuming the number of $(m + 1)$-layer blocks to be plotted along the vertical direction and the number of m-layer blocks along the horizontal direction, any sequence consisting of the two types of blocks is thus imaged as a zigzag path on this 2D lattice. The sequence which best approximates a uniform distribution of vacancy layers is then represented by the zigzag line which fits best the straight line S of which the slope is given by the ratio of the total length of the block sequences along the two directions; i.e. (Fig. 2),

$$\tan\varphi = (m + 1)q/mp \quad \text{or} \quad mp\tan\varphi - (m + 1)q = 0. \quad [12]$$

The two equations [11] and [12] are homogeneous in p

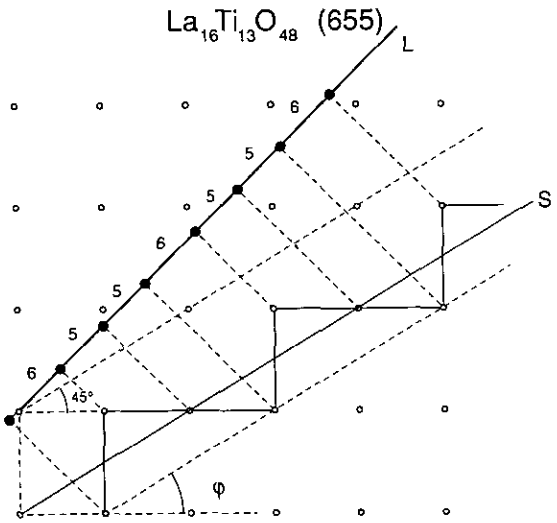

FIG. 2. "Cut and projection" method applied to the derivation of the stacking sequence 655 in $La_{16}Ti_{13}O_{48}$.

and q. The condition under which they have a nontrivial solution for p and q is then given by

$$\begin{pmatrix} (n/\delta) - m & (n/\delta) - (m+1) \\ m \tan\delta & -(m+1) \end{pmatrix} = 0,$$

which leads to an expression for $\tan\varphi$

$$\tan\varphi = -\{[(n/\delta) - m]/[(n/\delta) - (m+1)]\} \times [(m+1)/m]. \quad [13]$$

This relation determines the slope of the straight line S for any given value of δ and n, the value of m being determined by the double inequality (1). These relations are valid for any value of δ, including nonintegral or irrational values. If δ is irrational the resulting sequence will not be periodic. Complicated sequences of two kinds of rational blocks may thus result for arbitrary δ values. The actual stacking sequence is obtained by projecting the zigzag line on the line L enclosing an angle of 45° with the horizontal (Fig. 2) (18).

7. INTERPRETATION METHODOLOGY OF THE DIFFRACTION PATTERNS

The application of a variant of the "cut and projection" method (18) makes it possible to deduce not only the stacking sequence but also the essential features of the diffraction patterns for given values of n and δ. The method consists in making a cut by drawing two parallel lines with a slope φ through the 2D lattice considered above, based on a rectangular unit mesh of $m \times (m+1)$ units (see Fig. 2). The width of the cut or "slit" is determined by the requirement that the bordering lines pass through two diametrically opposed points of the basic rectangle. The block sequence is represented by the zigzag path described on points of this 2D lattice and confined by the "strip" or "slit" boundaries. The slit is half open; i.e., only points situated on one of the two lines, conventionally chosen, are accepted (Fig. 2).

As an example we deduce the sequence leading to the composition $La_{16}Ti_{13}O_{48}$. One has $n = 16$, $\delta = 3$, $m = 5$, and hence $m + 1 = 6$; i.e., the 2D lattice consists of rectangles of 5×6 units. The slope of the slit is given by $\tan\varphi = 6/10$. The actual sequence is now obtained by projecting the zigzag segments on a line L with a slope of 45°. From Fig. 2 it follows that the sequence must be 655655. . . . Since in this case δ is a small integer the sequence is finite and short.

The diffraction pattern is obtained by the transforma-

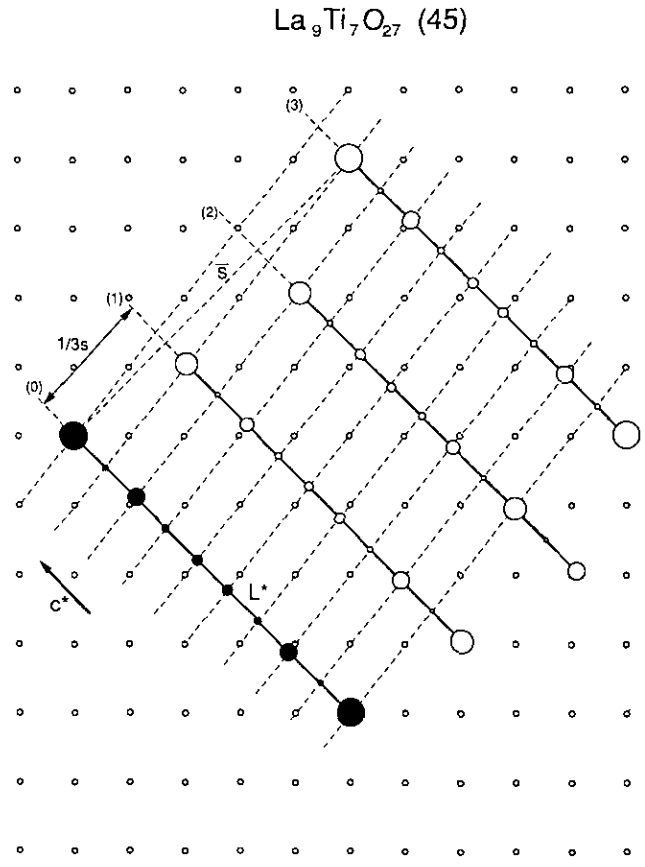

FIG. 3. Graphical method to determine the approximate relative intensity distribution in the diffraction pattern of $La_9Ti_7O_{27}$. The central row of diffraction spots is represented by the black dots; the noncentral rows are represented by open circles. The relative positions of the three rows are arbitrary; they are not representative of the geometry observed in the diffraction pattern; only the intensity distribution in the rows is relevant.

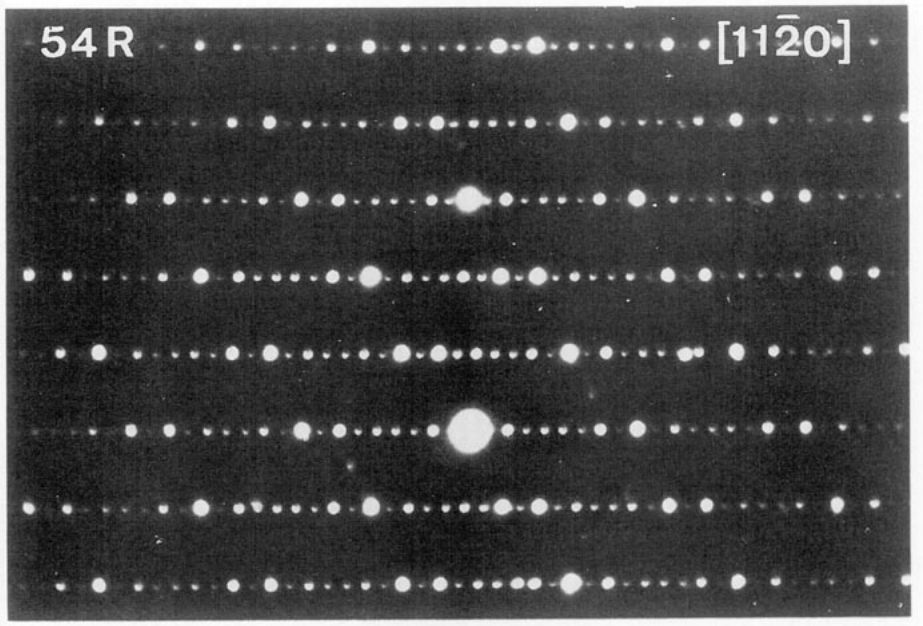

FIG. 4. Diffraction pattern along the [10$\bar{1}$0] zone of the phase $La_9Ti_7O_{27}$; this pattern can be compared with Fig. 3.

tion to Fourier space of the different operations giving rise to the strip. The construction of the central row of the diffraction pattern for the compound $La_9Ti_7O_{27}$, using the algorithm described in Refs. (18, 21), is represented in Fig. 3. The relative intensities of the diffraction spots, represented by dots of different sizes along L* in Fig. 3, are well reproduced because they are mainly determined by the geometry and size of the blocks, rather than by their detailed content, provided all blocks have the same average specific scattering power, which is the case here. The absolute intensities, however, do depend on the atoms present in the blocks. Figure 4 is the corresponding experimental diffraction pattern.

The diffraction pattern reveals directly the average spacing between vacancy layers since the separation of the first, relatively intense spot from the basic spot is given by δ/n; n is the number of intervals between the two basic spots, whereas δ is the number of intervals of this first relatively intense spot, counted from the closest basic spot ($n = 9$, $\delta = 2$ in Figs. 3 and 4).

In the generalized case where δ is not an integer the first intense spot still gives the average separation of the vacancy layers. The structure is now in fact an interface modulated structure with modulation wave vector $q = \delta/n$. The diffraction pattern may look incommensurate and exhibit spacing anomalies even though the "modules" are commensurate. The above mentioned algorithm for the construction of sequences then leads to possibly nonperiodic, but "uniform" sequences having a well defined long range order and thus producing sharp diffraction spots. If the first intense spot, which determines the q-vector, is separated from the basic spot by p intervals, the repeat unit contains p blocks. Figure 5 shows for instance the pattern to be expected for the 556 sequence in $La_{16}Ti_{13}O_{48}$. The distance between two basic spots (corresponding to the thickness of a single layer of 0.22 nm)

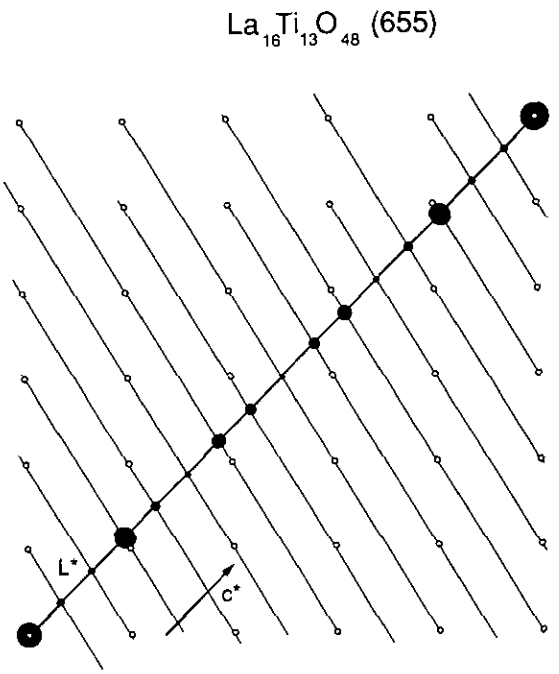

FIG. 5. Theoretical diffraction pattern (central row) of the phase $La_{16}Ti_{13}O_{48}$ using the "cut and projection" method.

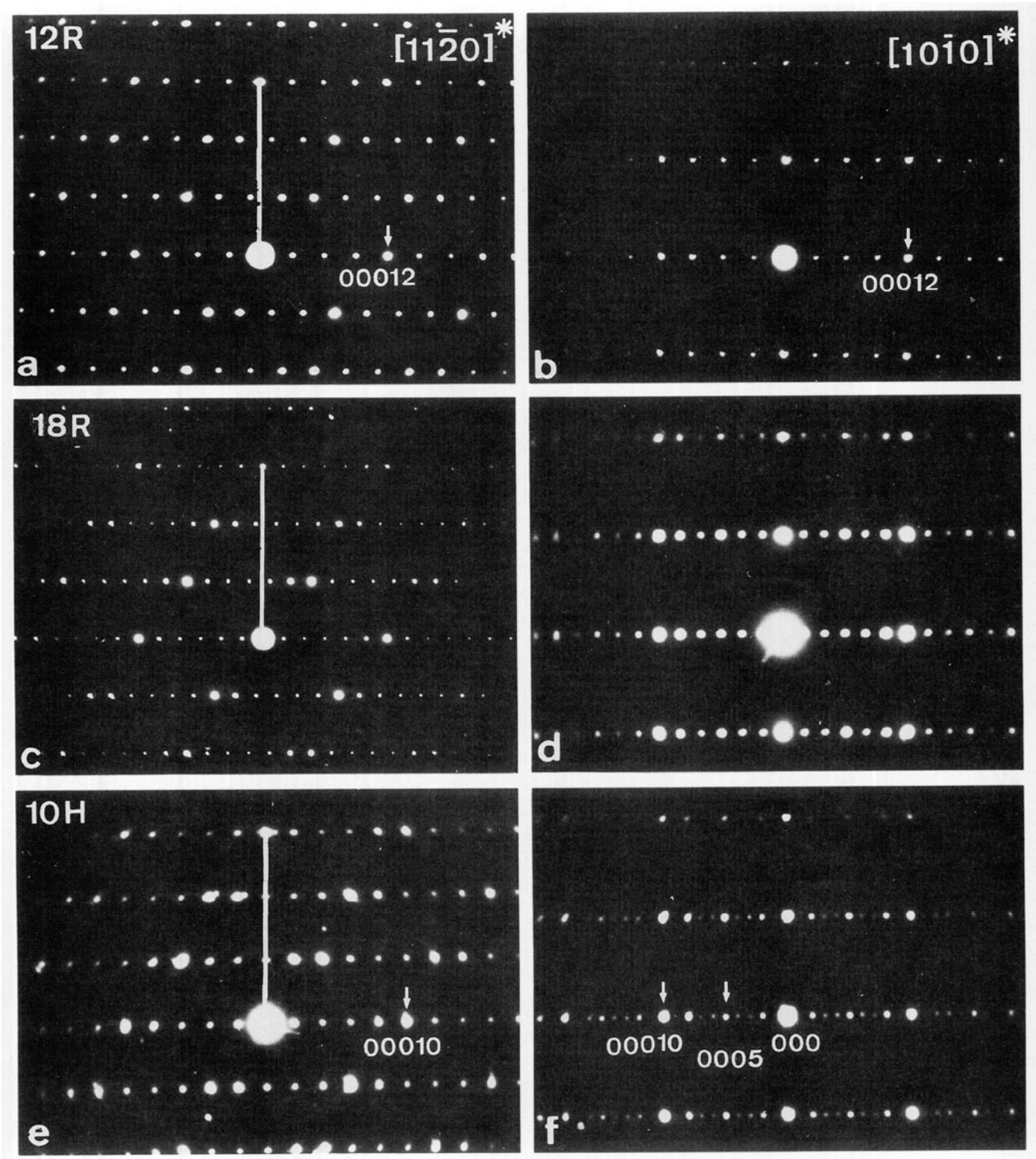

FIG. 6. Diffraction patterns of three monoblock polytypoids with $n = 4$, 5, and 6. The left column refers to the [11$\bar{2}$0] zone, whereas the right column refers to the [10$\bar{1}$0] zone. (a)(b) $La_4Ti_3O_{12}$ (12R); (c)(d) $La_6Ti_5O_{18}$ (18R); (e)(f) $La_5Ti_4O_{15}$ (10H).

is separated into 16 intervals and the first intense spot is separated by three intervals from the basic spot.

In Fig. 3, which refers to the compound $La_9Ti_7O_{27}$ with stacking sequence 45, the first intense spot is separated from the basic spot by two intervals. In single block sequences the spot intensity decreases in a monotonous manner with the separation from the basic spot; Fig. 6 shows, for instance, the diffraction patterns for the compounds 4, 5, and 6.

The diffraction pattern thus allows the direct determination of δ and n and hence of m; i.e., of the two block sizes. Since these parameters in turn determine the slope of the slit, the block sequence is also determined directly.

In the case n = threefold − 1 the blocks are stacked vertically and the vacancy layers define the blocks. In the cases n = threefold + 1 and threefold the successive blocks are, moreover, shifted over a vector $\mathbf{R} = \frac{1}{3}[11\bar{2}0]$. This results in a parallel shift of the intersection line L* in the diagram of Fig. 3, simulating the fractional shift of the noncentral superlattice spot sequences with respect to the basic spot positions (22). The fractional shifts $\mathbf{g} \cdot \mathbf{R}$ are the same for all spots along a row parallel to c^*; the components along the layer plane of the corresponding diffraction vectors are the same and thus the dot product $\mathbf{g} \cdot \mathbf{R}$ is also the same since $\mathbf{R}$ is a vector in the layer plane. A lateral shift of L* which results in the desired fractional shift of the dot pattern can be obtained as follows. A parallel shift of L* over $\mathbf{s}$, where $\mathbf{s}$ is a reciprocal lattice vector of the 2D lattice, brings the line L* again through a node of this lattice; it only results in a parallel shift of the resulting dot pattern, which is not an essential change. However, a displacement of L* over the fraction $\mathbf{g} \cdot \mathbf{R}$ of $\mathbf{s}$ causes the desired fractional shift and now produces the spot sequences along noncentral rows. In the present case the fractional shifts are $\pm\frac{1}{3}$ (mod 1). A possible construction is shown in Fig. 3; it is clear that any other lattice vector s of the 2D-lattice could have been chosen, leading to the same final result.

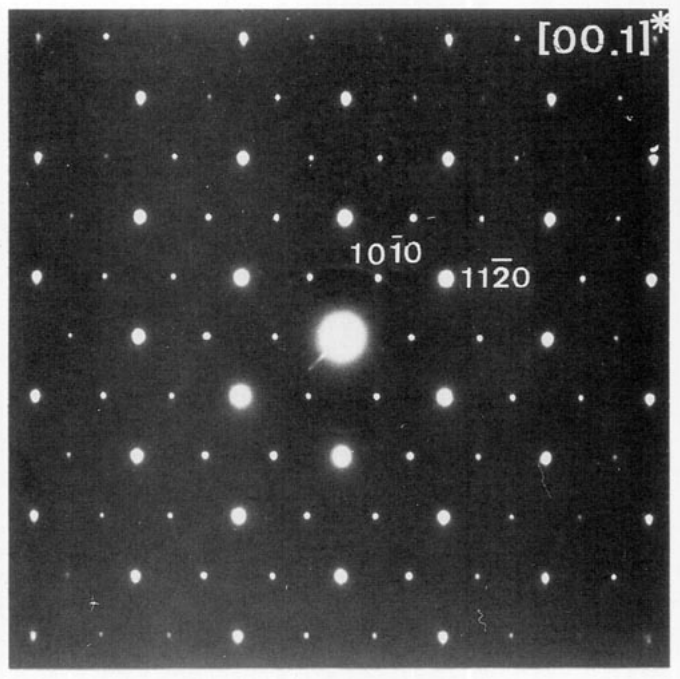

FIG. 7. The [0001] zone diffraction pattern of the series of phases $La_nTi_{n-1}O_{3n}$. Note the two levels of intensity of the diffraction spots.

8. OBSERVED DIFFRACTION PATTERNS

We shall first discuss the diffraction patterns due to the simplest phases, i.e., those containing one type of repeat unit only.

The 5H (10H) Phase (n = 5; δ = 1) (Fig. 6e,f, Fig. 7)

The diffraction pattern along the c^* zone of Fig. 7 consists of a hexagonal array of spots corresponding to a lattice parameter a_H = 0.557 nm in agreement with the geometry of the LaO_3 layers. The spots belong to two classes of intensities; the set of the most intense spots forms a two-dimensional hexagonal lattice with lattice parameter $a_H^*/\sqrt{3}$. These intense spots reflect the fact that the projected arrangement of the La ions forms a hexagonal array with lattice parameter $a_H\sqrt{3}$, confirming the structure of the LaO_3 layers and their stacking.

The most relevant diffraction patterns are those along the $[11\bar{2}0]^*$ and $[10\bar{1}0]^*$ zone; they are shown in Fig. 6. In Fig. 6 the spacing between the most intense (basic) spots, indicated by arrows, corresponds with the layer thickness 0.22 nm of one LaO_3 layer. In the 5H diffraction patterns (Fig. 6e) this basic spacing is divided in five intervals. The intensity of the spots decreases monotonically with their separation from the basic spots. They form rectangular meshes, i.e., they are aligned along normals to c^*. The most intense basic spots in successive spot rows systematically occupy shifted positions along the c^* direction (the shift increasing with increasing h); this reflects the predominantly ABC . . . stacking of the layers.

Tilting experiments about the c^* axis reveal that the c-spacing is in fact 2 × 1.096 nm; i.e., it contains 10 LaO_3 layers. This can be deduced from the diffraction patterns of Fig. 6f in which the interspot spacing is only half of that observed along the $[11\bar{2}0]^*$ zone pattern. This 10-layer spacing is exhibited in all zones of the type $[hki0]^*$ except for the three symmetry-related $[11\bar{2}0]^*$ type zones. We conclude that the following diffraction conditions are satisfied:

$h\bar{h}0l$ is present for l = even

and

$000l$ for l = even.

This latter condition is derived from the observation that the $000l$ spots for l = odd are only present if these spots are also present in non-central rows of reflections. Their presence in the $[10\bar{1}0]^*$ zone type patterns must be attributed to double diffraction.

The observed diffraction conditions are consistent with two trigonal space groups $P3c1$ (*nr* 158) and $P\bar{3}c1$ (*nr* 165) and with three hexagonal space groups $P6_3cm$ (*nr* 185), $P\bar{6}c2$ (*nr* 188) and $P6_3/mcm$ (nr 193).

It is worth noting that the intensity distribution in rows of spots parallel to c* in the $[10\bar{1}0]^*$ zone pattern, can be accounted for by assuming the structure to be composition modulated. The basic structure must then have a prominent double layer period (due to deformation) as viewed along this zone and it must further be composition modulated by a five-layer superperiod. Since 5 and 2 have no common factor the real period becomes ten layers. The most intense diffraction spots are then the "basic" spots with $l = 0$, $l = 5$ and $l = 10$. The other spots have then to be considered as satellites of these basic spots, with a **q**-vector $\mathbf{q} = \frac{1}{5}\mathbf{c}_H^*$, their intensity decreasing with their separation from the basic spots.

Alternatively one obtains the same set of reflections if one considers the structure as having a basic period of c = 1.1 nm, i.e., equal to the thickness of five layers, further commensurately modulated by a deformation wave with a wave vector $\mathbf{q} = 2.5\mathbf{c}^*$ (corresponding to two layer thicknesses). The two descriptions are equivalent, but it is more customary to consider the shortest period as the basic one and the larger one as the modulation period.

The 18R Phase ($n = 6$, $\delta = 1$)

The $(0001)^*$ basal section is not very different from that of the 5H phase above. The geometry and the intensity distribution of the spots are the same. Only the nodes of the type $h\bar{h}0l$ with h = threefold are touched by Ewald's sphere, but the nodes $h\bar{h}01$ and $h\bar{h}0\bar{1}$ ($h \neq 3$) are close enough to Ewald's sphere, i.e., at $\pm\frac{1}{3}c^*$, to produce spots due to relrods.

Since the structure is rhombohedral successive spot positions along rows in the $[11\bar{2}0]^*$ zone diffraction pattern are shifted along c^* over $h \times \frac{1}{3}c^*$; the spot spacing corresponds to the thickness of 6 LaO_3 layers (Fig. 6c,d).

In the $hh\bar{2}\bar{h}l$ spot rows, i.e., in the $[1\bar{1}00]^*$ zone, the period remains equal to the thickness of six layers. The spot with $l = 3$ is relatively more intense, which again reflects the presence of a prominent double layer period, when viewed along this zone. Since the composition modulation period of six layers is a multiple of the 2-layer deformation period, the actual period remains 6, at variance with the case $n = 5$ where period doubling occurs. There are no systematic extinctions.

The 12R Phase ($n = 4$, $\delta = 1$)

The 12R diffraction patterns are rather similar "mutatis mutandis" to those of the 18R phase (Figs. 6a,b). The rhombohedral shift along c^* over $\pm\frac{1}{3}$ of the $h\bar{h}il$ spot positions is also visible here (Fig. 6a). The interspot spacing now corresponds to the thickness of 4-layers. Along the $hh\bar{2}\bar{h}l$ spot rows the interspot spacing remains the same (Fig. 6b); there is again no period doubling (due to the tilt of the octahedra as we shall see below) since n = 4 is even. The c_H-parameter contains $3 \times 4 = 12$ layers, due to the rhombohedral lattice.

The 54R Phase ($n = 9$, $\delta = 2$)

The diffraction pattern of this phase along the $[11\bar{2}0]^*$ zone is reproduced in Fig. 4. The separation of the basic spots (corresponding with the thickness of one LaO_3 layer) is divided into nine equal intervals by the diffraction spots. The first intense spot, counted from the basic spots is the second one; this means that $\delta = 2$ and the composition is thus $La_9Ti_7O_{27}$. The modulation vector is $q = \frac{2}{9}c^*$. Using the "cut and projection method" described above the block sequence corresponding with this value of q is 45. Also, the theoretical diffraction pattern can be constructed by the same method. The relative spot intensities are found to correspond remarkably well with the observed ones (Fig. 3). Since n = odd the real period contains 54 layers.

The 78R Phase ($n = 13$, $\delta = 3$)

As an example of the analysis of a complex phase, exhibiting all the characteristic features of this family of mixed layer structures, we discuss in some detail the patterns made along the $[11\bar{2}0]^*$ and $[10\bar{1}0]^*$ zone (Figs. 8a and b).

In Fig. 8a the distance between two successive basic spots, indicated by arrows, is divided into 13 equal intervals. Since 13 = threefold + 1 the structure is rhombohedral and successive $hh\bar{2}\bar{h}l$ spot rows suffer a $\pm\frac{1}{3}$ shift, as indicated by the vertical lines in Fig. 8a. The first intense spot in the $h\bar{h}00$ row counted from the basic spot is the third one, i.e., $\delta = 3$. The composition is therefore $La_{13}Ti_{10}O_{39}$ and the block sequence must contain three blocks. From the location of the first intense spot we find the values $q = \frac{3}{13}$ and $\tan\varphi = \frac{5}{8}$. From this we can deduce the block sequence by means of the cut and projection method; it is found to be 445. Also, the theoretical diffraction pattern can be deduced graphically; the result is shown in Fig. 9. The relative intensities of the spots are

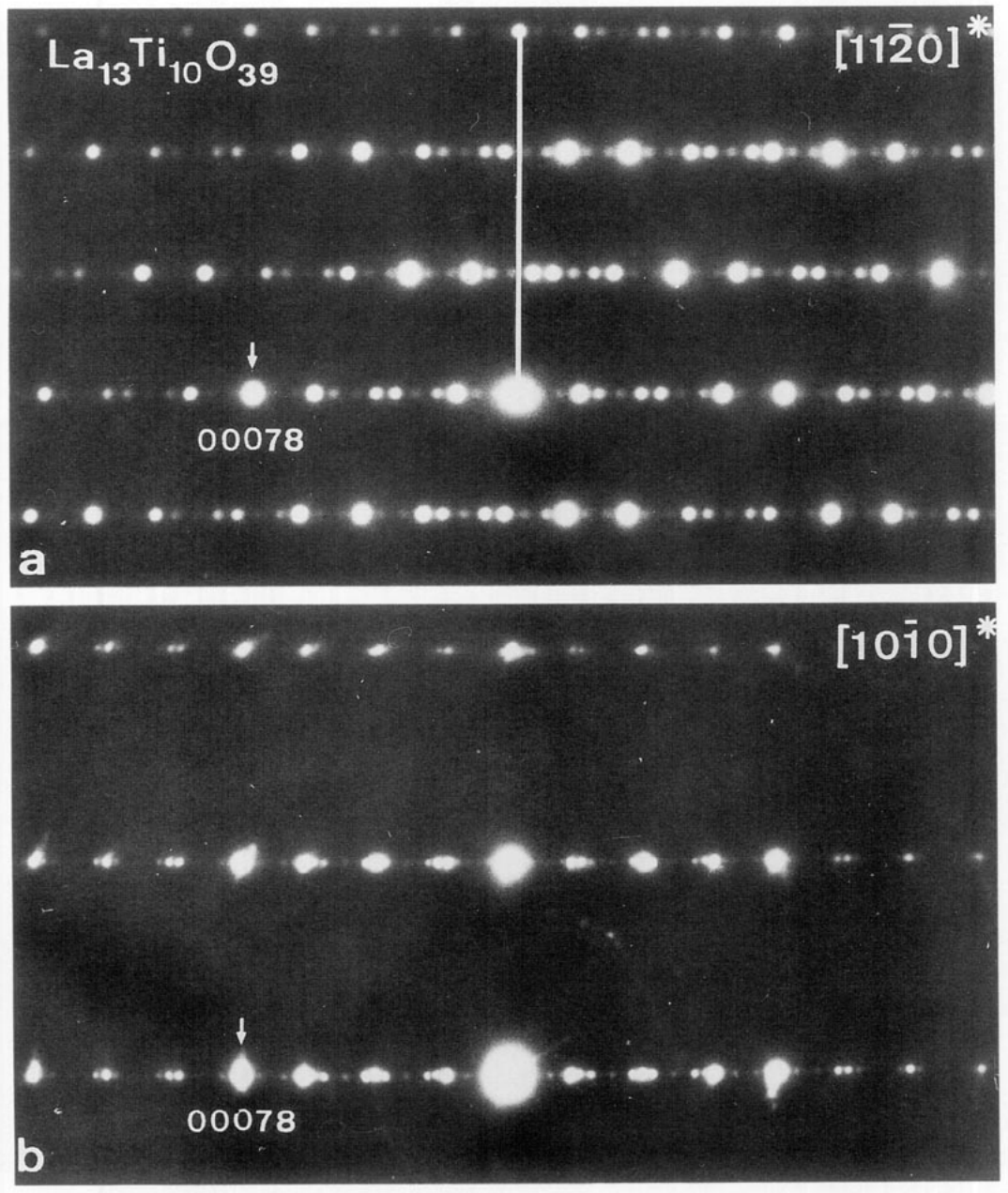

FIG. 8. Diffraction pattern of the phase $La_{13}Ti_{10}O_{39}$ (78R): (a) $[11\bar{2}0]^*$ zone; (b) $[10\bar{1}0]^*$ zone.

quite well reproduced, as can be judged by comparing with Fig. 8a.

In the $[10\bar{1}0]^*$ zone (Fig. 8b) the interspot spacing is only half that in the $[1120]^*$ zone, showing that the c-parameter must be doubled, as a consequence of the tilt pattern of the TiO_6 octahedra, in agreement with the fact that $n = 13$ is odd. The total c-parameter is thus equal to a $13 \times 3 \times 2 = 78$ layer thickness.

An "Incommensurate" Pattern with $q = 11/46$

Figure 10 shows an apparently incommensurate diffraction pattern along the $[11\bar{2}0]^*$ zone. The q-value deduced from the first intense spots is approximately $q = 11/46$. Since $4 < 46/11 < 5$ the sequence consists of 4 (m) and 5 ($m + 1$) layer blocks, but neither n nor δ is directly measurable from the diffraction pattern.

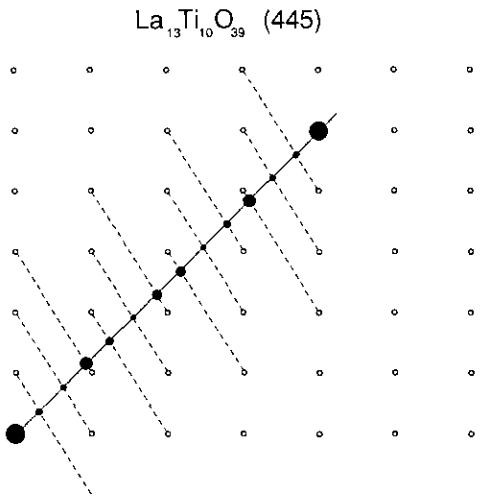

FIG. 9. Theoretical diffraction pattern of the phase $La_{13}Ti_{10}O_{39}$ (78R), which can be compared with the observed pattern of Fig. 8a.

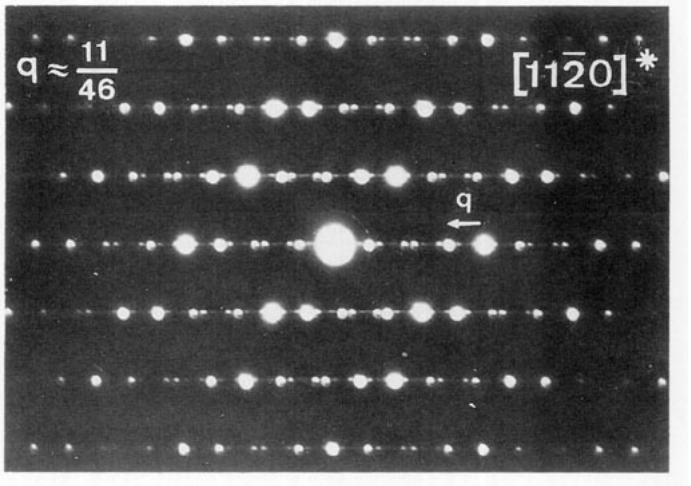

FIG. 10. "Incommensurate" diffraction pattern with a wavevector $q \approx 11/46$. Note the spacing anomaly. The corresponding stacking sequence can be approximated by 4444544. . . .

However, we know that the average spacing $n/\delta = 1/q = 46/11$. From formula (12) we can thus deduce that $\tan \varphi = 10/36$. The corresponding stacking sequence is 4444544. It is close to pure 4 with a 5 block inserted quasiperiodically.

9. HIGH RESOLUTION IMAGES

The high resolution images made along the zones [11$\bar{2}$0]* and [10$\bar{1}$0]* confirm the structures proposed in the previous paragraphs.

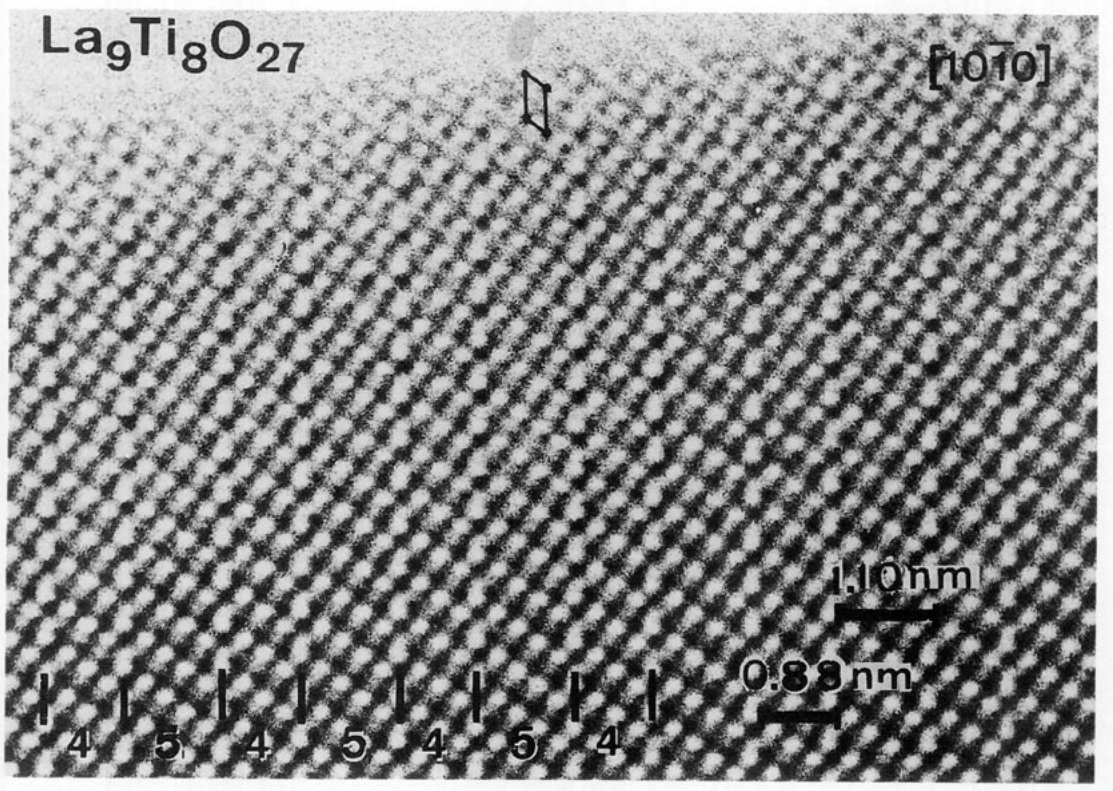

FIG. 11. High resolution image along the close packed directions of the polytypoid 45. In the thin part of the wedge-shaped sample the dark dots represent lanthanum columns and the grey dots titanium columns. The projected unit cell of the basic structure is outlined. This image can be compared with Fig. 1d.

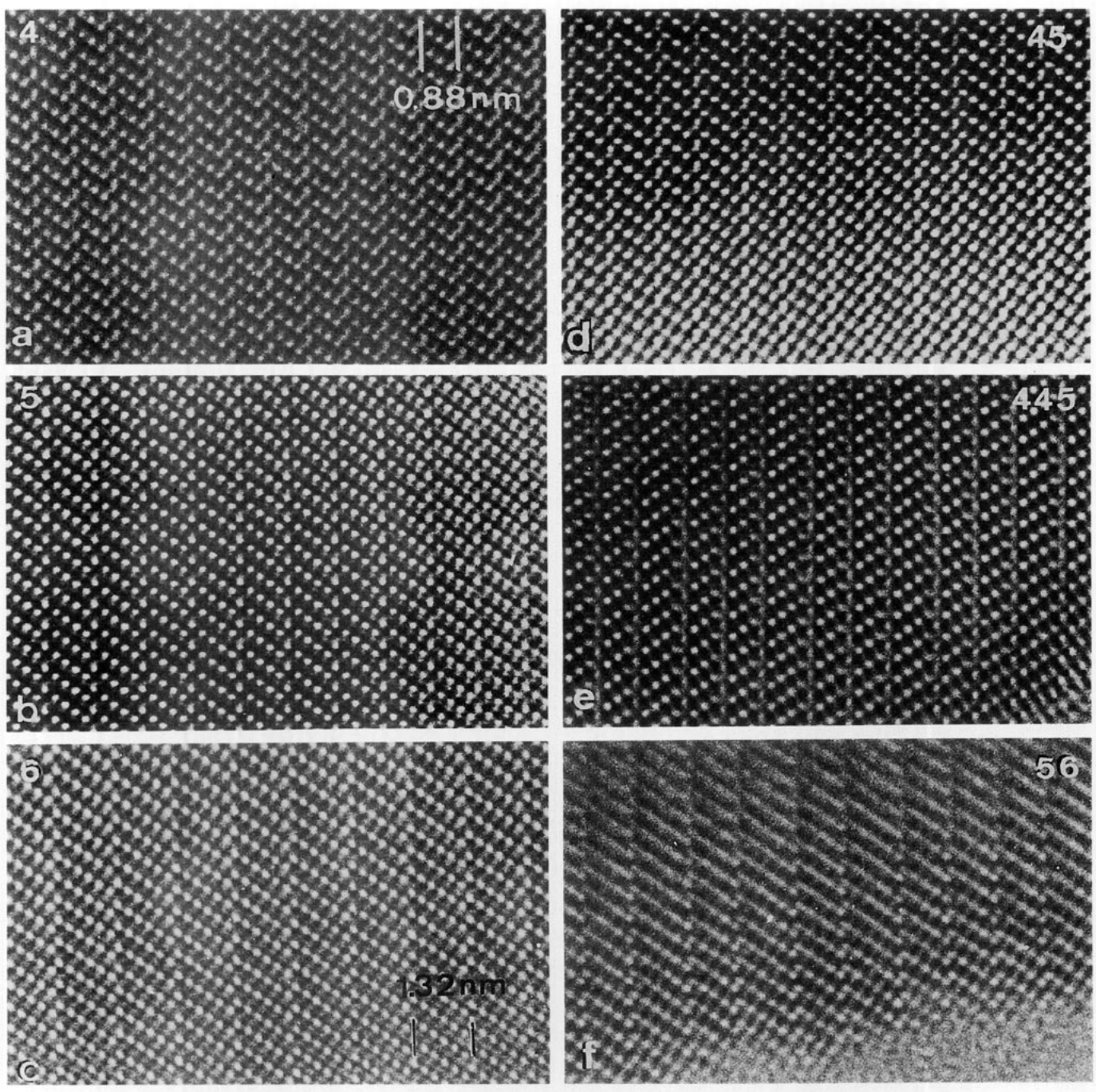

FIG. 12. High resolution images of different polytypoids along the close packed directions (a) $La_4Ti_3O_{12}$ (12R) 4; (b) $La_5Ti_4O_{15}$ (10H) 5; (c) $La_6Ti_5O_{18}$ (18R) 6; (d) $La_9Ti_7O_{27}$ (54R) 45; (e) $La_{13}Ti_{10}O_{39}$ (78R) 445; (f) $La_{11}Ti_9O_{33}$ (12R) 56.

The most informative high resolution images are those along zones parallel to the close packed directions of the layers. The crystal structure of the compound $La_5Ti_4O_{15}$ as viewed along such a close packed direction is represented in Fig. 1d. The projected lanthanum positions form a 2D parallelogram shaped network, which is the projection of a 3D network of flattened octahedra; it is indicated by double lines in Fig. 1d. The titanium positions project in the centres of these parallelograms; they are indicated by medium sized round dots in Fig. 1. The oxygen atoms are indicated by small dots and the vacancy rows by squares. Oxygen positions are usually not revealed in high resolution images.

Figure 11 is an image along such a zone of a crystal

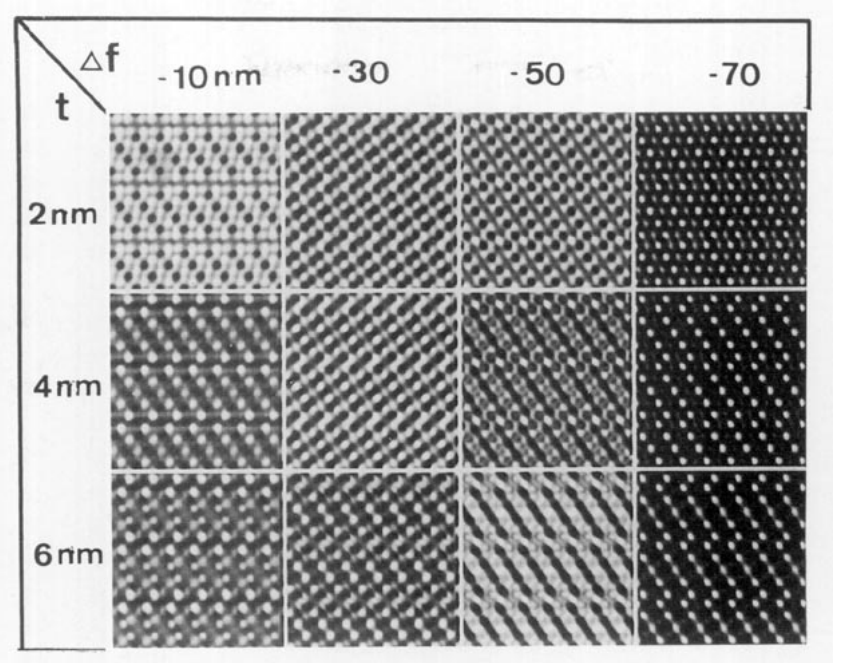

FIG. 13. Matrix of calculated HR images along [11$\bar{2}$0] of the 18R structure for different defocus values (horizontal) and different thicknesses (vertical).

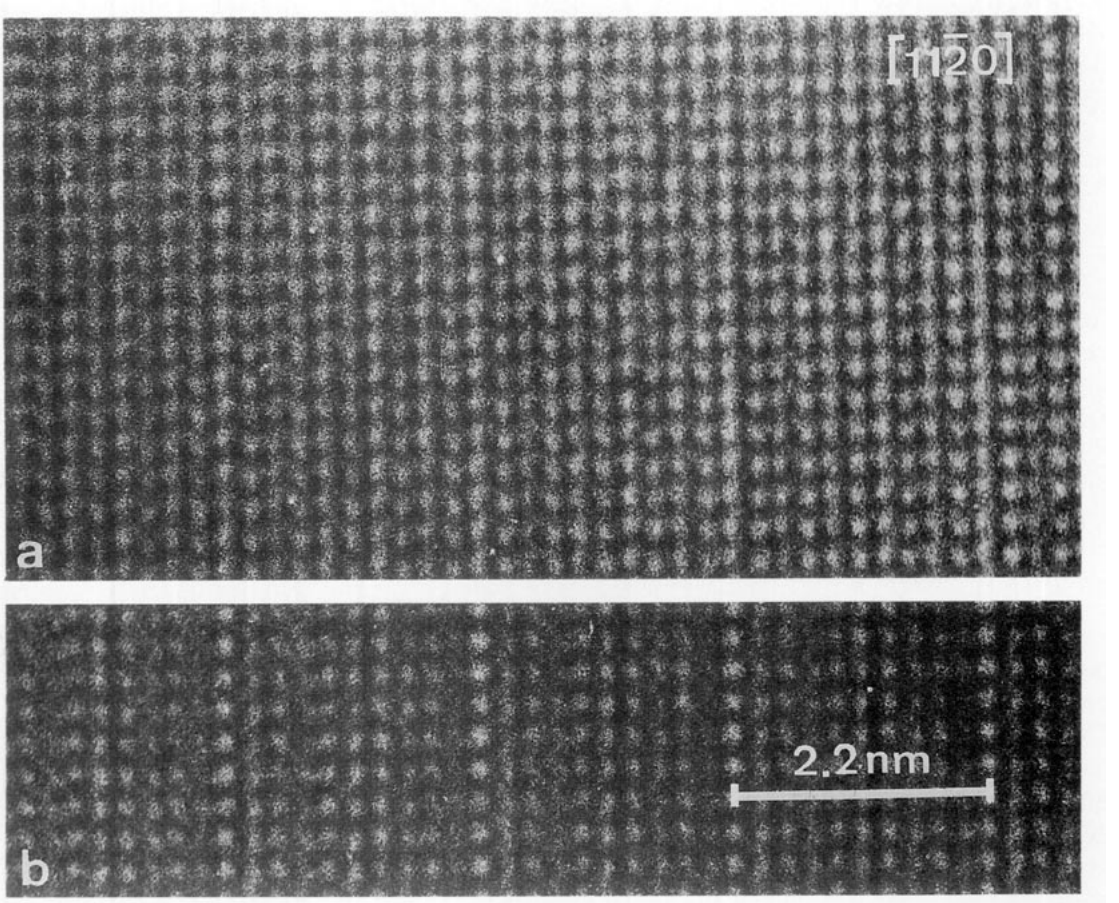

FIG. 14. [1120] high resolution image of the 10H polytypoid ($La_5Ti_4O_{15}$): (a) thin area; (b) thicker area. The c-axis is horizontal.

fragment of $La_9Ti_7O_{27}$; the correspondence with the projected structure is indicated schematically using the same symbols as in Fig. 1d. It is obvious that the structure contains 4- and 5-layer blocks in accordance with the model that follows from considerations discussed above.

In the $[11\bar{2}0]^*$ zone image the structure is viewed along the close packed rows of the LaO_3 layers. Close to the thin edge of the foil the La-containing columns are marked by pronounced dark dots, whereas the titanium containing columns are imaged as grey dots. As usual, pure oxygen columns are not revealed. In thicker parts of the foil only the lanthanum-containing columns are clearly revealed as bright dots (Fig. 14). A number of images of different polytypoids are reproduced in Fig. 12.

This image interpretation follows directly from the symmetry of the image and from the one to one correspondence of dots and projected structure. It was confirmed by the computer simulations of the image based on the described model. The images were computed for a wide range of thicknesses and defocus values; a matrix for $n = 6$ is reproduced in Fig. 13.

The $[10\bar{1}0]^*$ zone image is less informative (Fig. 14), but it strikingly confirms the structure, as is evident from a comparison with the projected model of Fig. 15. According to the idealized structure, all atom columns are now aligned along the c-direction, but the vacancy layers causing the superperiod can still be recognized.

The array of bright dots in Fig. 14 (10H-phase) has roughly the geometry, i.e., the size and shape, of the array of columns containing lanthanum and oxygen, as viewed along the $[10\bar{1}0]$ zone. However, the array is not rectangular, as one would expect for the idealized structure (Fig. 15). The rows along the c-axis are slightly zigzag shaped. In the space groups under consideration ($P3c1$, $P\bar{3}c1$) the positions of the lanthanum atoms are determined by symmetry; i.e., they are situated on the trigonal axis, and the rows of lanthanum columns should therefore be straight and parallel to c. However, the zigzag arrangement of the bright dots can be understood by noting that in the actual model the oxygen octahedra are slightly rotated, as discussed in Section 10. The oxygen atoms the projected positions of which coincided with those of the lanthanum columns in the ideal structure are hereby slightly shifted alternatingly to the left and to the right in successive rows, as indicated at the top of Fig. 15. The extrema in lattice potential, which give rise to the bright dots, are hereby shifted as well, due to the eccentric, albeit small contribution of the oxygen columns.

The zigzagging in Fig. 14 is established objectively by digitized averaging over 10 frames, followed by computer generation of lines of equal brightness (Fig. 16). The elongated shape of the dots is consistent with our assumption that they are formed by the superposition of straight rows of lanthanum columns and of oxygen columns displaced alternatingly left and right in a direction perpendicular to c.

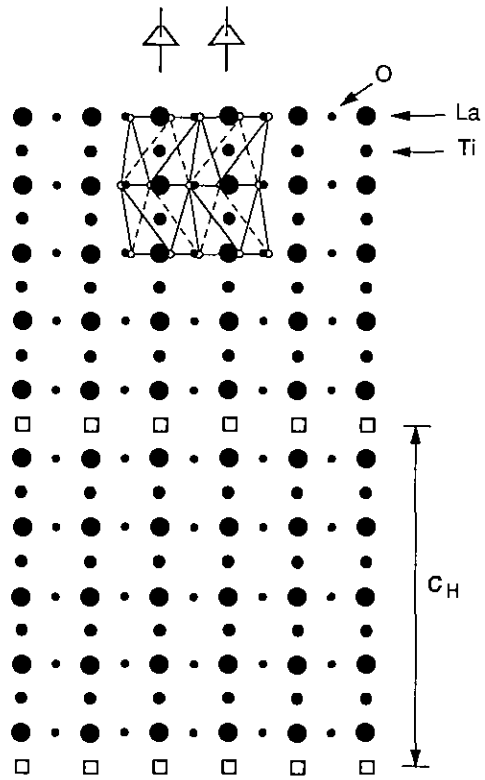

FIG. 15. Projection of the idealized 10H structure along the $[11\bar{2}0]$ zone. In the upper part the displacements of the oxygen atoms associated with the tilt of the TiO_6 octahedra is shown schematically.

10. MODELS FOR THE SUPERSTRUCTURES

The structure models described above (Sections 3 and 4) are idealized in the sense that the TiO_6 octahedra are implicitely assumed to be perfectly regular. They correctly represent the topological features of the structures, but the real structures are more complicated as a result of small deformations. We describe in detail the model for the 10H phase, the other structures being built on the same principles.

It is well known that below a certain temperature the regular TiO_6 octahedra become unstable in many structures; they may become deformed, the titanium ions occupying often eccentric positions in the octahedra. This is, for instance, the case in tetragonal $BaTiO_3$ and in a number of titanates derived from the perovskite structure.

From the diffraction patterns we concluded that the prominent period as seen along the close packed directions is equal to the thickness of one LaO_3 layer. In projection along the $[11\bar{2}0]^*$ zone on the other hand the promi-

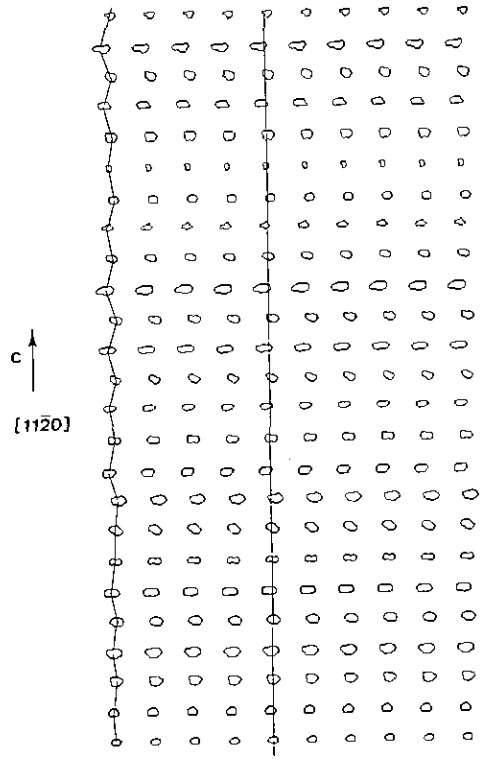

FIG. 16. Equi-intensity contours of a digitized averaged high resolution image of the type shown in Fig. 14.

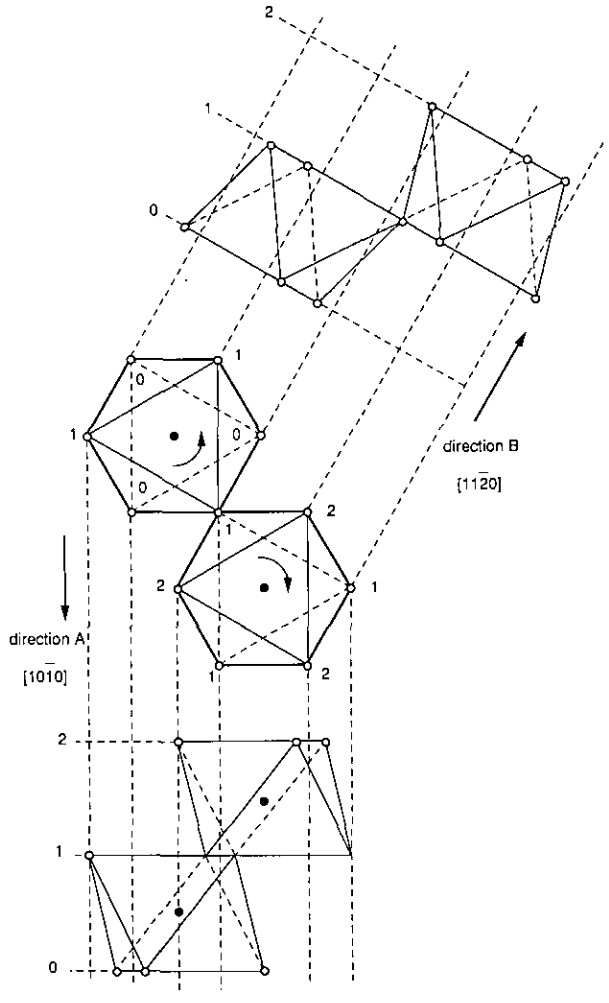

FIG. 17. Coupling of corner-sharing octahedra in the $La_nTi_{n-1}O_{3n}$ structure: direction A: along the close-packed direction; direction B: perpendicular to the close-packed direction.

nent basic period becomes equal to the thickness of two layers. This causes the spots with $l = 5$ (mod 10) to be relatively more intense than the other superstructure spots.

Assuming the period doubling to be due to deformation of the TiO_6 octahedra, the displacement pattern should be consistent with the presence of three (six) fold rotation symmetry about an axis normal to the layer planes and it should conserve the unit mesh in the c-plane, but should double the c-parameter.

Any tilt pattern of corner-sharing octahedra about a tilt-axis which is not parallel to the c-axis breaks the trigonal (hexagonal) symmetry and can thus be excluded. It is therefore compelling to assume that the deformation of the TiO_6 octahedra must result from a small tilt about the c-axis. Such a tilt leads to flattening of the coupled octahedra. The unit mesh in the layer plane being conserved, all TiO_6 octahedra situated in the same c-layer planes must be tilted in the same sense and by the same small angle. Each TiO_6 octahedron is "enclosed" in a strongly flattened octahedron formed by six lanthanum ions, limited by the same layers as the TiO_6 octahedra. These lanthanum octahedra share edges and thus form a rigid framework within which the TiO_6 octahedra apparently have only a very limited tilt possibility (Fig. 1).

In the cubically stacked part of the structure the TiO_6 octahedra share corners; as a result successive c-layers of octahedra are rotated in opposite senses and the basic period normal to these layers is doubled. This is shown schematically in Fig. 17. The octahedra of the hexagonal triplet are face-sharing and hence the octahedra in adjacent c-layers, in this part of the structure, are tilted in the same sense.

A deformed version of the structure of the 10H-phase resulting from the described tilt pattern is reproduced in Fig. 18a,b. The shaded octahedra in (b) are situated in the same plane, parallel to the plane of the drawing, which passes through the titanium ions, situated in the centers of the octahedra, i.e., passing through the threefold rotation axis.

A front as well as a side view are represented in Fig.

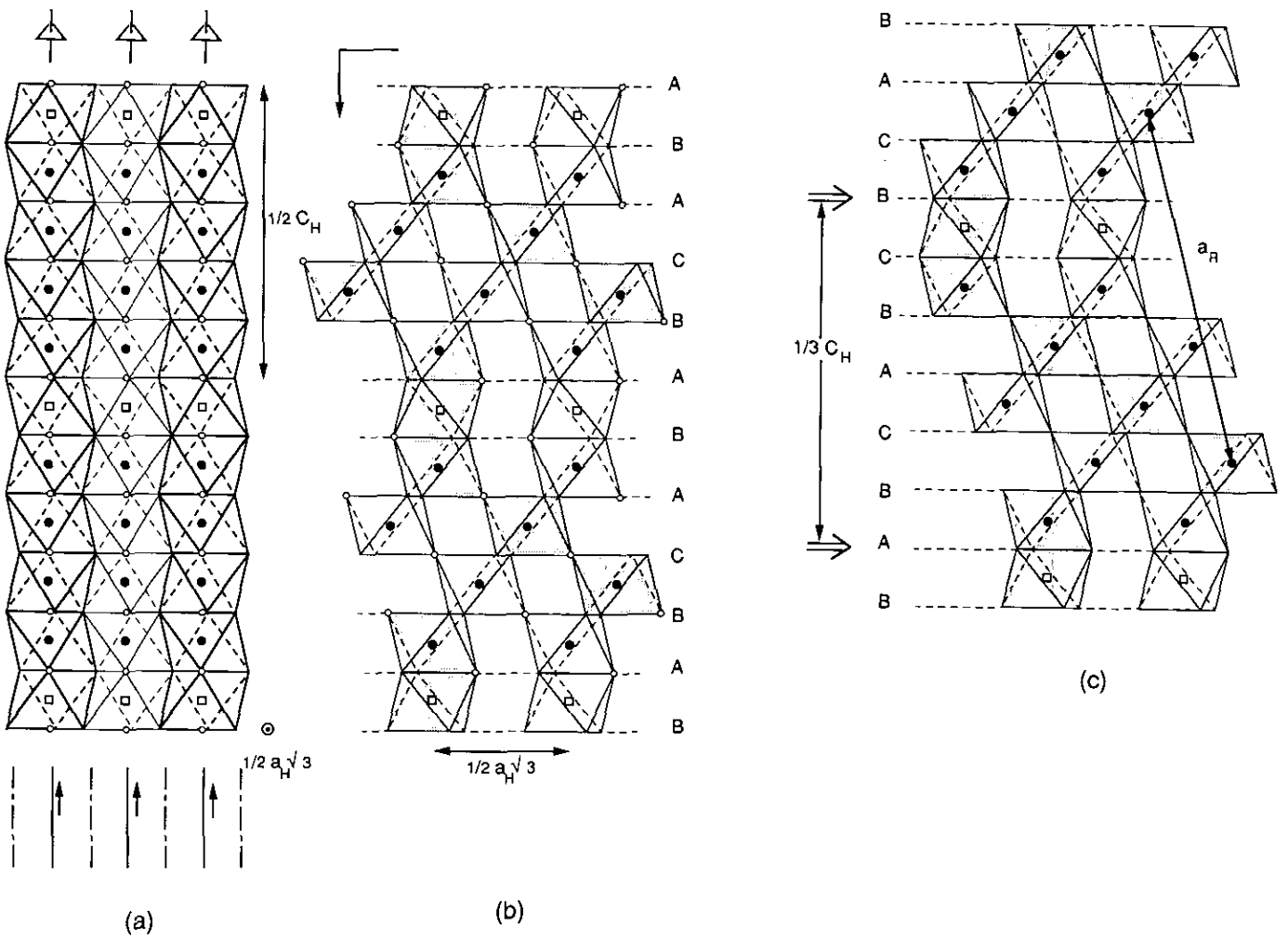

FIG. 18. Schematic representation of the real structure of 10H: (a) View along the [11$\bar{2}$0] zone. Note the zigzag arrangement of the oxygen atoms. A prominent two-layer period is obvious. The symmetry elements are indicated schematically. (b) View along the [10$\bar{1}$0] zone. The shaded octahedra are situated in the same plane. A glide mirror plane is parallel to the plane of the drawing. (c) View of the real structure of 18R along the [10$\bar{1}$0] zone. The plane of the drawing is not a glide-mirror plane.

18 a and b. When ignoring the difference between full (front) and dotted (rear) lines i.e. in projection, the period along the c-direction is equal to the thickness of five layers (1.1 nm) (Fig. 18b). However when taking into account front and rear part of the octahedra we note that a displacement of $c_H/2$ (1.1 nm) along the c-direction, followed by a reflection with respect to the plane parallel to the plane of the drawing and passing though the titanium ions, is a symmetry operation, i.e., this plane is a glide mirror plane with a $c_H/2$ glide vector. This can also be concluded from the side view of the structure shown in Fig. 18a. The same conclusion can be reached for the symmetry related planes. The space group of this model structure thus contains three sets of glide mirror planes enclosing angles of 60°, intersecting along the rows of titanium ions which are situated on the threefold rotation axis.

One can similarly conclude that diagonal glide mirror planes are present halfway between the axial glide mirrors. The two spacegroups $P3c1$ and $P\bar{3}c1$ are consistent with this model and with the diffraction conditions. The other three space groups mentioned before are not consistent with the model because they contain mirror planes, while the model does not.

It is also evident from the side view of Fig. 17a that a prominent period equal to the thickness of two layers results. This bilayer sequence is composition modulated by a period equal to five layers, leading to a tenfold period.

The principal of the deformation pattern is the same in the other structures. It should be noted that the presence of the glide mirror plane, i.e., of the extinctions for l = odd, depends on the parity of the number of layers in the repeat unit. For instance, when the repeat unit is six layers

thick, there is no period doubling; moreover, the structure is rhombohedral: 18R (Fig. 18c).

The simple rules that make it possible to conclude whether a structure is rhombohedral or hexagonal, and hence whether or not the c-parameter has to be tripled, can be extended to include the effect of the deformation pattern on the lattice parameter along the layer normal.

The rhombohedral (R) or hexagonal (H) type depends on the value of n (mod 3), whereas the doubling of the lattice parameter resulting from the octahedron tilts depends on n (mod 2). As a result, the following four combinations can occur. If the resulting structure is rhombohedral and n = even, the lattice parameter is three times the thickness of the repeat unit (e.g., $n = 6$); if n = odd it is six times the thickness of the repeat unit (e.g., 445). If, on the other hand, the resulting structure is hexagonal and n = even the lattice parameter is equal to the thickness of the repeat unit, but for n = odd it is the double (e.g. $n = 5$).

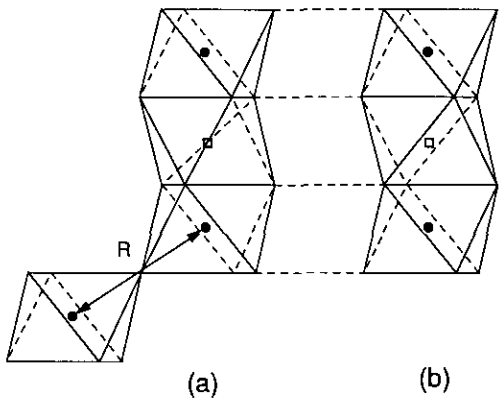

FIG. 20. Structure model viewed along the [11$\bar{2}$0] zone: (a) illustrating the deformation of an octahedron in the contact plane between two crystal parts in which the octahedra are deformed in opposite senses; (b) normal structure of the hexagonal triplet in the structure.

11. PLANAR DEFECTS

In a number of high resolution images defects, imaged as pronounced dark lines, are present (Fig. 19). They always coincide with the positions of the stacking fault planes, in particular with the hexagonal triplets adjacent to the isolated block layer; for instance, adjacent to the 5-block in a sequence 4445 (Fig. 19). They are only easily visible in the thicker parts of wedge shaped specimens.

Although an extensive set of simulated images was generated for the perfect crystal, albeit ignoring the small rotations of the octahedra, no image comparable with the pronounced dark lines was obtained. It is therefore concluded that these lines must image planar faults associated with the hexagonal triplets.

An unambiguously established model cannot be proposed at present, but it is possible to speculate on probable ones. It should be noted that "a priori" two senses of rotation of the TiO_6 octahedra about the c-axis are equally probable. Since these rotations are coupled there is a strong tendency to have the same consistent pattern of corner sharing octahedra in large crystal parts. However, where, on transforming into a ferroic phase, the rotations

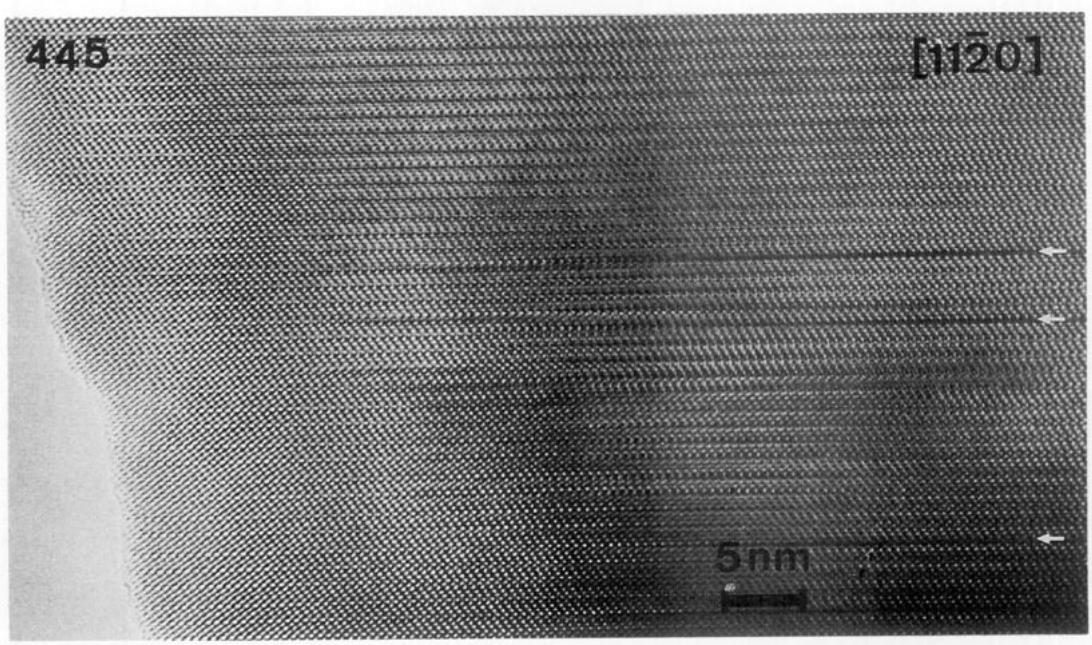

FIG. 19. High resolution image of the 445 phase. Note the presence of extra dark lines imaging planar interfaces located in (0001).

start independently in different parts of the crystal, they may be incompatible where different domains meet. Rotation patterns of opposite sense would not lead to a different image along the close packed rows, as in Fig. 20, since the projected lattice potential is the same. Domains would thus not be obvious in such images. It is not unreasonable to assume that the contact plane between two oppositely rotated regions would coincide with the layers of empty octahedra, which is the most easily deformable one, and which as a result would become distorted by a twist about the c-axis (Fig. 20). This twist would also locally change the layer spacing and hence change the contrast. Such an interface could be called a "rotational anti-phase boundary" since the tilt patterns on both sides are in anti-phase. The relationship between blocks on either side of the interface can alternatively be described as a translation over a vector **R** (Fig. 20a) which has a component parallel to the layer plane.

In some places quasiperiodic arrangements of such boundaries occur (Fig. 19); their separation being the same as the period of the idealized structure. This is consistent with the proposed model since the fault planes are assumed to be associated with the hexagonal triplet adjacent to the layer of singular blocks, which determines the period.

The diffraction patterns along the [1010]* zone of specimens containing several such faults exhibit diffuse streaking halfway between the spot rows (Fig. 21). We believe that this diffuse scattering is caused by the planar defects discussed here. The streaks have reinforcements corresponding to the spacing between successive layers, showing that even in faulted regions a strong correlation in the tilt pattern between successive layers of octahedra is maintained.

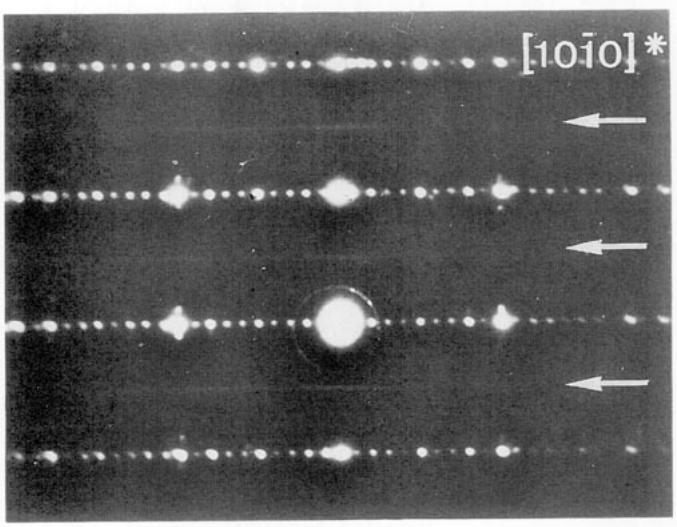

FIG. 21. Diffraction pattern along the [11$\bar{2}$0] zone of the 10H phase. Note the relatively strong intensity of the spots with I = 5. Halfway between the spot rows weak diffuse streaks are observed.

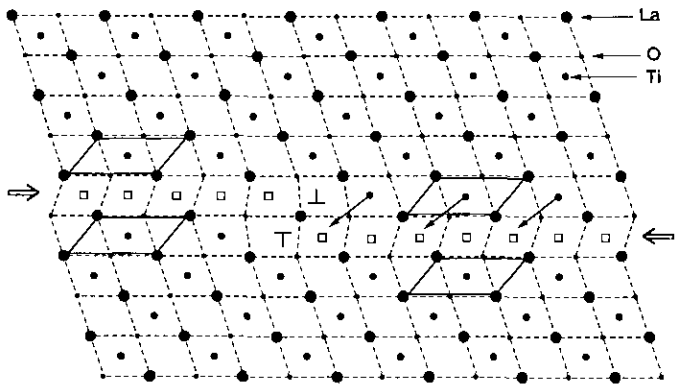

FIG. 22. Model of the defect responsible for the mobility of the vacancy layers in the hexagonal quadruplet of layers. The defect consists of a dipole of stair rod dislocations of the vacancy type.

In Ref. (23) it was shown that disorder in the tilt pattern of octahedra in the cubic perovskite structure leads to diffuse streaks along the cube directions passing through the reciprocal lattice point $\frac{1}{2}, \frac{1}{2}, \frac{1}{2}$ and to diffuse cube planes. In the present case the streaks are parallel to c^*.

An alternative explanation, which we consider to be less probable however, consists in assuming that the dark lines are in fact defects of the type described below, i.e., steps in the fault plane, the dipoles being by chance parallel to the foil surface over a large number of unit cells. In view of the small thickness of the sample this is rather improbable, however.

Occasionally isolated defects occur in the stacking sequences; they usually consist of a single block of the wrong size, for instance a single 4-layer block in a sequence of 5-layer blocks.

Sometimes also defects of a different nature are found; for instance, a 54 lamella becoming gradually a 45 lamella, the rest of the structure being unaffected. At such a defect the level of the hexagonal quadruplet changes by one layer; as a consequence the vacancy layer is also stepped. Such a line defect is represented as viewed edge on in Fig. 22; it can formally be described as a dipole of partial "stair-rod" type dislocations. This defect can be either of the vacancy or of the interstitial type. A [11$\bar{2}$0] zone view of such a defect is shown in Fig. 23; it can be compared with the schematic one of Fig. 22, where it is assumed that the dipole is of the vacancy type. Defects of this type are possibly frozen-in "leftovers" from the mechanism responsible for the rearrangement of the block sequences. The propagation of the dislocation dipole by glide along the (0001) layer plane, accompanied by the cooperative rearrangement of the titanium ions, results in the widening of one block by one layer at the expense

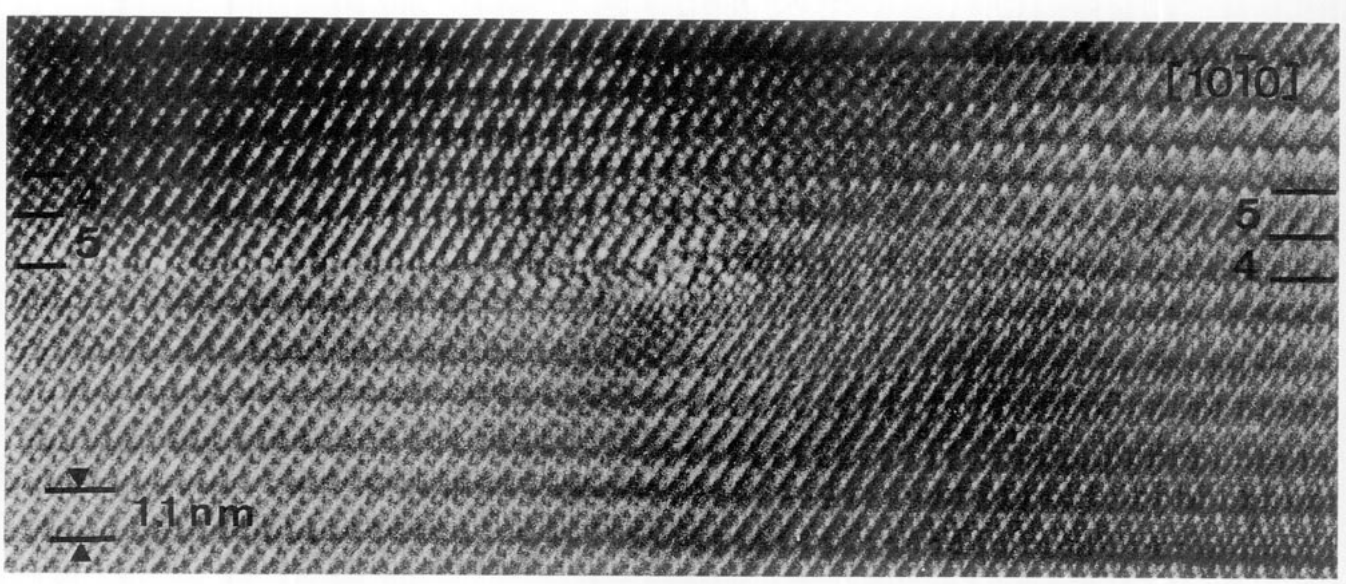

FIG. 23. High resolution image suggesting the presence of a defect of the type illustrated in Fig. 22.

of the corresponding narrowing of the adjacent block. During this motion the titanium ions only have to jump into vacancies in the adjacent vacancy layer. Rearrangement of the block sequences can thus take place easily at moderate temperatures since only very short range diffusion of the titanium ions, coupled with the conservative motion of a dislocation dipole, are required. Such a mechanism allows us to understand the formation of the surprisingly long sequences of perfectly ordered complex block sequences.

12. DISCUSSION

The structures of the compounds $La_5Ti_4O_{15}$ and $La_9Ti_7O_{27}$ which were determined by means of X-ray powder diffraction (24) have been confirmed by electron diffraction and high resolution electron microscopy. Moreover, it was found that the building principle of these structures can be generalized to a large series of homologous compounds of the general chemical composition $La_n Ti_{n-\delta}O_{3n}$.

Our observations have in particular demonstrated the direct relationship between composition and stacking sequence in the system $La_nTi_{n-\delta}O_{3n}$. High resolution images make it possible to "read" directly the local stacking sequences. The sequence corresponding to the theoretical, average, composition is always the most abundant one, but often not the only one; slightly different sequences are usually formed as well. This happens more often for the complicated multiblock sequences than for the simpler monoblock sequences. For instance sequences such as 4445 and 445 were found in neighbouring parts of the same sample. The sequence variability is attributed to small inhomogeneities in the composition of the samples; very long heat treatments would be required to produce perfectly ordered structures with such long periods.

The physical origin of long period structures is still a matter of debate. Depending on the type of material different driving forces for long period interface ordering have been proposed. A model derived from the ANNNI model (25), originally developed for magnetically ordered structures, has been successfully applied to a certain class of long period antiphase boundary modulated alloys. The model assumes competing interactions of opposite sign between first and second nearest neighbors along one direction. It has been applied to long period alloy structures containing periodic conservative antiphase boundaries such as Cu_3Pd (27), Al–Ti (28), Au–Zn (29), and Cu–Al (30). However in certain alloys the antiphase boundaries are nonconservative and the structures are mainly composition driven; this is, for instance, the case for the Au–Mn (31) and the Ni–Mo systems (32).

Also, in the present materials, the formation of the long period structures is undoubtedly composition driven since the observed sequences depend directly on the chemical composition. Variations in the stacking sequences within the same crystal fragment are presumably due to slight inhomogeneities in the composition; the materials may not have been completely equilibrated.

The formation of complicated sequences such as 4445 can be understood in terms of the following simple qualitative picture. The composition, and in particular the Ti^{3+}/Ti^{4+} ratio determines the average separation of the inter-

faces (i.e., of the layers of titanium vacancies). The absence of positive titanium ions along the interfaces causes some net charge localized along these interfaces and hence leads to a repulsive Coulomb type interaction between successive parallel interfaces. The interaction law is presumably of the shielded Coulomb type. The equilibrium configuration of a set of parallel interfaces, interacting by repulsive forces, which decrease faster than linear with the interface separation, is the equidistant arrangement (see appendix). However, due to the discrete nature of the lattice, the interface separation can only adopt values which are integer multiples of the interlayer spacing. Very often the average separation imposed by the composition will not be such an integer multiple. The best approximation to an equidistant distribution is then the sequence obtained by the "cut and projection" method described above. This algorithm produces "uniform" sequences which have a well defined long range order and therefore produce a diffraction pattern have a well defined long range order and therefore produce a diffraction pattern consisting of sharp spots. The physical realization of the uniform sequences could proceed by the mechanism described above (Section 9.2).

13. CONCLUSIONS

The materials with composition $La_nTi_{n-\delta}O_{3n}$ were shown to form a homologous series of polytypoids or mixed layer compounds having either hexagonal or rhombohedral symmetry. Their structures can be derived from that of cubic perovskite by introducing periodically intrinsic faults with a displacement vector $\frac{1}{3}[1\bar{2}10]_H$ in the cubic stacking of close packed LaO_3 layers, leading to stacking sequences of the type hcc . . . ch. The octahedral interstices formed exclusively by oxygen ions are occupied by titanium ions, except for the central layers of octahedral in the hexagonal triplets associated with the stacking faults, which remain empty, making up for the nonstoichiometry. The number n is equal to the number of LaO_3 layers in the repeat unit if $\delta = 1$. If $\delta > 1$ the period contains δ repeat units (or blocks) of two different thicknesses. The following block sequences were observed in high resolution images made along the close packed directions: 4, 5, 6, 45, 445, 4445, 56. More complicated sequences such as 44545 were deduced from the diffraction patterns. All observed sequences are uniform, i.e., they exhibit long range order and thus produce sharp diffraction spots. The sequences, as well as all semiquantitative features of the diffraction pattern can adequately be analyzed graphically using the cut and projection method.

All compounds for which n is odd exhibit period doubling. It was shown that the superperiod is due to tilting of the octahedra about the c-axis accompanied by deformation. The tilt pattern occurs in all polytypoids, but it gives rise to the presence of glide mirror planes only if n is odd. The tilting and period doubling are confirmed by high resolution imaging along the $[10\bar{1}0]$ zone.

The deformation of the TiO_6 octahedra makes it possible to explain in a natural and consistent manner the occurrence of glide mirror planes leading to extinctions in the diffraction patterns of the different phases and in particular the dependence on the parity of n.

Like many other titanates, the materials studied here are presumably ferroic, either ferroelastic, ferroelectric, or both, and transform into the idealized phases at the critical temperature. If this is confirmed the space group would be unambigeously defined as $P3c1$ (No. 158). High temperature electron diffraction experiments are under way to verify the presence of this phase transition.

APPENDIX

Whatever be the interaction law, a sufficient condition for equilibrium is that each interface in the sequence of identical repelling interfaces should be symetrically surrounded by similar parallel interfaces; i.e., an interface at X must be surrounded by interfaces at $X \pm x_1$; $X \pm (x_1 + x_2)$; $X \pm (x_1 + x_2 + x_3)$; . . . ; $X \pm (\Sigma x_j)$. The same must of course apply to any other interface of the sequence and in particular to the interfaces at $X + x_1$. This implies that the interfaces at $(X + x_1) - x_1$ and at $(X + x_1) + x_2$, as well as those at $(X + x_1) - (x_1 + x_2)$ and at $(X + x_1) + (x_2 + x_3)$, should be located symmetrically with respect to the interface at $X + x_1$. This implies that $/x_1/ = /x_2/$; $/x_2/ = /x_3/$; . . . ; i.e., the separation between successive interfaces must be constant.

A sufficient equilibrium condition is intuitively clear; however, it is possible to prove analytically that it is also a necessary condition for the case whereby the interaction is assumed to be proportional to the inverse of the interface separation. It is also assumed that the interfaces are sufficiently numerous to allow a description in terms of an interface density function $D(x)$ such that $D(x)\,dx$ represents the number of interfaces in the interval $x, x + dx$, where x is chosen perpendicular to the interfaces. We further assume that the interfaces are present in the interval $-a \leq x \leq +a$, i.e., the average density is $N/2a$. The force exerted on an interface at X, $-a \leq X \leq +a$, is then proportional to

$$\int D(x)\,dx/(X - x) = 0. \qquad [1]$$

The integral equation (1) has a solution

$$D(x) = (n/\pi)/(a^2 - x^2)^{1/2},$$

where use was made of the normalization condition that the interval $-a$, $+a$ contains n interfaces. This expression would for instance describe the interface distribution in a crystal with a finite thickness $2a$ along the c-direction, where the surfaces act as barriers for the outer interfaces of the sequence. However, in practice, we observe only a small fraction of a long sequence, somewhere in the central part of the crystal. We are therefore more interested in a situation where n and $2a$ both go to infinity in such a way that the ratio $n/2a$ remains constant and equal to the average interface density, whereas x remains finite; under these conditions $D(x)$ becomes a constant, i.e., the interfaces separation is constant, confirming the intuitive reasoning.

REFERENCES

1. D. A. MacLean, H. N. Ng, and J. E. Greedan, *J. Solid State Chem.* **30,** 35 (1979).
2. F. Lichtenberg, D. Widmer, J. G. Bednorz, T. Williams, and A. Reller, *Z. Phys. B* **82,** 211 (1991).
3. F. Queyroux, M. Huber, and R. Collongues, *C. R. Acad. Sci. Paris* **C240,** 806 (1970).
4. J. K. Drandon and H. D. Megaw, *Philos. Mag.* **21,** 189 (1970).
5. M. Gasperin, *Acta Crystallogr.* **31,** 2129 (1975).
6. R. Portier, M. Fayard, A. Carpy, and J. Galy, *Mater. Res. Bull.* **9,** 371 (1974).
7. R. J. D. Tilley, *in* "Chemical Physics of Solids and Their Surfaces" (M. W. Roberts and J. M. Thomas, Eds.), Chap. 6, p. 121. Royal Soc. Chem. Great Britain, 1980.
8. T. Williams, H. Schmalle, A. Reller, F. Lichtenberg, D. Widmer, and G. Bednorz, *J. Solid State Chem.* **93,** 534 (1991).
9. D. A. MacLean and J. E. Greedan, *Inorg. Chem.* **20,** 1025 (1981).
10. W. D. Johntson and D. Sestrick, *J. Inorg. Nucl. Chem.* **20,** 32 (1961).
11. M. German and L. M. Kovba, *J. Inorg. Chem.* **28,** 2377 (1980).
12. H. J. Rother, S. Kemmler-Sack, U. Treiber, and W. R. Cyris, *Z. Anorg. Allg. Chem.* **466,** 131 (1980).
13. A. Galasso and L. Katz, *Acta Crystallogr.* **14,** 647 (1961).
14. R. Bontchev, F. Weill, and J. Darriet, *Mater. Res. Bull.* **27,** 931 (1992).
15. S. Kemmler-Sack, *Z. Anorg. Allg. Chem.* **461,** 146 (1980).
16. S. Kemmler-Sack and U. Treiber, *Z. Anorg. Chem.* **462,** 166 (1980).
17. H. M. Rietveld, *J. Appl. Crystallogr.* **2,** 65 (1969).
18. V. Elser, *Phys. Rev. B* **32,** 4892 (1985), *Acta Crystallogr. Sect. A* **42,** 36 (1986).
19. M. Duneau and A. Katz, *Phys. Rev. Lett.* **54,** 2688 (1985).
20. N. Frangis, S. Kuypers, C. Manolikas, G. Van Tendeloo, J. Van Landuyt, and S. Amelinckx, *J. Solid State Chem.* **84,** 314 (1990).
21. S. Amelinckx, C. Van Heurck, and G. Van Tendeloo, *in* "Quasi-Crystals and Incommensurate Structures in Condensed Matter," Proc. Third International Meeting on Quasi-Crystals Mexico (M. J. Yacaman, D. Romen, V. Castano, and A. Gomez, Eds.), p. 300). World Scientific, Singapore, 1989.
22. J. Van Landuyt, R. De Ridder, R. Gevers, and S. Amelinckx. *Mater. Res. Bull.* **5,** 353 (1970).
23. M. Verwerft, D. Van Dyck, W. A. M. Brabers, J. Van Landuyt, and S. Amelinckx, *Phys. Status Solidi: A* **112,** 451 (1989).
24. R. Bontchev, B. Darriet, J. Darriet, F. Weill, G. Van Tendeloo, and S. Amelinckx, *Eur. J. Solid State Inorg. Chem.* **30,** 521 (1993).
25. R. J. Elliot, *Phys. Rev.* **124,** 346 (1961).
26. D. de Fontaine and J. Kulik, *Acta Metall.* **33,** 145 (1985).
27. D. Broddin, G. Van Tendeloo, J. Van Landuyt, S. Amelinckx, and A. Loiseau, *Philos. Mag. B* **57,** 31 (1988).
28. A. Loiseau, G. Van Tendeloo, R. Portier, and F. Ducastelle, *J. Phys. (Paris)* **46,** 595 (1985).
29. D. Broddin, G. Van Tendeloo, and S. Amelinckx, *J. Phys. Condens. Matter* **2,** 3459 (1990).
30. D. Broddin, G. Van Tendeloo, J. Van Landuyt, and S. Amelinckx, *Philos. Mag.* **59,** 179 (1989).
31. G. Van Tendeloo and S. Amelinckx, *Phys. Status Solidi: A* **43,** 553 (1977); **65,** 73 (1981); and **65,** 431 (1981).
32. G. Van Tendeloo and S. Amelinckx, *Phys. Status Solidi: A* **22,** 621 (1974); G. Van Tendello, J. Van Landuyt, P. Delavignette, and S. Amelinckx, *Phys. Status Solidi: A* **25,** 697 (1974); and G. Van Tendeloo, P. Delavignette, J. Van Landuyt, and S. Amelinckx, *Phys. Status Solidi: A* **26,** 299 (1974).